DOKUZ EYLÜL UNIVERSITY
GRADUATE SCHOOL OF NATURAL AND APPLIED SCIENCES

QUANTUM MONTE CARLO INVESTIGATIONS OF QUANTUM DOTS

by

Aylin YILDIZ

July, 2009
İZMİR

QUANTUM MONTE CARLO INVESTIGATIONS OF QUANTUM DOTS

A Thesis Submitted to the
Graduate School of Natural and Applied Sciences of Dokuz Eylül University
In Partial Fulfillment of the Requirements for the Degree
of Doctor of Philosophy in
Physics

by

Aylin YILDIZ

July, 2009
İZMİR

Ph.D. THESIS EXAMINATION RESULT FORM

We have read the thesis entitled **"QUANTUM MONTE CARLO INVESTIGATIONS OF QUANTUM DOTS"** completed by **AYLİN YILDIZ** under supervision of **PROF. DR. İSMAİL SÖKMEN** and we certify that in our opinion it is fully adequate, in scope and in quality, as a thesis for the degree of Doctor of Philosophy.

.....

Prof. Dr. İsmail SÖKMEN

Supervisor

.....	.....
Prof. Dr. Kadir YURDAKOÇ	Prof. Dr. Fevzi BÜYÜKKILIÇ
Thesis Committee Member	Thesis Committee Member
.....	.....
Examining Committee Member	Examining Committee Member

Prof. Dr. Cahit HELVACI
Director
Graduate School of Natural and Applied Sciences

ACKNOWLEDGEMENTS

It is delight to acknowledge all the people who have supported me over my Ph.D. study.

First of all I wish to express my greatest appreciation and thanks to my supervisor Prof. Dr. İsmail Sökmen for his excellent guidance, patience and continual encouragement. Many of the research subjects were initiated by Prof. Sökmen and he offered many constructive ideas to solve problems with physics as well as computational fields.

Special thanks go to Assis. Prof. Dr. Kadir AKGÜNGÖR for his advice and constructive criticism on earlier drafts of this thesis. Without his technical support this work would never have become what it is today.

Also I would express my thanks to Prof. Dr. Oğuz GÜLSEREN at Bilkent University for sharing invaluable knowledge about Density Functional Theory and its implementation via software package.

The days would have passed far more slowly without the support of my friends who shared their humor and encouraged me on this journey.

Finally, I wish to thank my parents for their unconditional love and support throughout my life.

Aylin YILDIZ

This thesis is dedicated to my mother and father.

QUANTUM MONTE CARLO INVESTIGATIONS OF QUANTUM DOTS

ABSTRACT

In this thesis, we have applied both the Variational Monte Carlo (VMC) and Monte Carlo Diagonalization (MCD) techniques for calculation the ground-state energies of correlated electron-hole pair (exciton) and interacting two electrons confined in a two dimensional (2D) disc-like and three dimensional (3D) spherical parabolic quantum dots. The effects of dimensionality and quantum confinement on the ground state as well as binding energies of a correlated electron-hole pair in parabolic quantum dots have been investigated. Moreover, under parabolic confinement potential and within effective mass approximation size and shape effects of quantum dots on the ground state energy of two electrons have been studied.

We have used four variational trial wave functions constructed as the harmonic-oscillator basis multiplied by different correlation functions. The relative performance of trial wave functions has been tested. It has been found that the variational wave functions which correlation part is constructed as a linear expansion in terms of Hylleraas-like coordinates significantly improve the desired results. Our results show that the proposed ansatz is able to capture nearly exactly the ground-state energies of excitons, and it properly account for the results of correlated two electrons in parabolic quantum dots.

Very few terms are needed to reach an accuracy comparable to more common wave function forms with large basis sets. The MCD technique puts no constrains on the potential as well as trial wave function and can be systematically improved by adding more terms using the procedure described.

Finally, this study indicates that Monte Carlo Diagonalization technique combined with the proposed trial wave function are a powerful tool for studying interacting particles in parabolic quantum dots.

Keywords: quantum dot, exciton, Variational Monte Carlo (VMC) method, Monte Carlo Diagonalization (MCD) method.

KUANTUM NOKTALARIN KUANTUM MONTE CARLO İNCELEMELERİ

ÖZ

Bu tezde, iki boyutlu (2D) disk benzeri ve üç boyutlu (3D) küresel parabolik kuantum noktalarda kuşatılan etkileşen iki elektron ve elektron-deşik çiftinin (ekziton) taban durum enerjilerini hesaplamak amacıyla Varyasyonel Monte Carlo (VMC) ve Monte Carlo Diagonalizasyon (MCD) yöntemleri uygulandı. Boyut ve kuantum kuşatmanın, parabolik kuantum noktalarda etkileşimli elektron-deşik çiftinin taban durumu ve bağlanma enerjileri üzerindeki etkileri incelendi. Ayrıca, parabolik kuşatma potansiyeli ve ektin kütle yaklaşımı dahilinde kuantum noktaların büyüklük ve şeklinin iki elektron üzerindeki etkileri araştırıldı.

Harmonik-osilatör bazı ile farklı korelasyon fonksiyonlarının çarpımı şeklinde oluşturan dört varyasyonel deneme dalga fonksiyonu kullanıldı. Deneme dalga fonksiyonlarının birbirine göre performansları test edildi. Korelasyon kısmı, Hylleraas-benzeri koordinatlar cinsinden oluşturulan varyasyonel dalga fonksiyonlarının incelenen sonuçları önemli ölçüde iyileştirdiği bulundu. Sonuçlar, önerilen dalga fonksiyonun parabolik kuantum noktalardaki ekzitonların taban durumu enerjilerini tam olarak oluşturduğunu ve benzer olarak etkileşen iki elektron için doğru veriler ürettiğini göstermektedir.

Az sayıda terim, daha popüler büyük baz setleri kullanılarak hesaplanan doğrulukta verilerin elde edilmesi için yeterlidir. MCD tekniği, potansiyel üzerine olduğu kadar deneme dalga fonksiyonu üzerinede herhangi bir kısıtlama oluşturmaz ve terim sayısı arttırılarak sistematik olarak iyileştirilebilir.

Sonuç olarak bu çalışma, Monte Carlo Diagonalizasyon metodu ile önerilen deneme dalga fonksiyonunun, parabolik kuantum noktalarda etkileşen parçacıkların incelenmesinde güçlü bir çözüm tekniği oluşturduğunu ortaya koymaktadır.

Anahtar sözcükler: kuantum nokta, ekziton, Varyasyonel Monte Carlo (VMC) metodu, Monte Carlo Diagonalizasyon (MCD) metodu.

CONTENTS

Page

CHAPTER ONE
INTRODUCTION

During the last 20 years a new research area in condensed-matter physics has been explored. More advanced experimental techniques allow for the possibility of artificial creation of low-dimensional quantum confined systems containing just a few electrons. Such small man-made artificial systems that confine electrons, holes, or electron-hole pairs or so called excitons to a small region on the order of the electrons' de Broglie wavelength are usually called quantum dots. The typical dimensions of quantum dots range nanometers to a few microns, and their size, shape and interactions can be precisely controlled through the use of advanced nanofabrication technology. The size tunability and unique optical and electrical properties of these "artificial atoms", that are different in character to those of the corresponding bulk material, enable never before seen applications to science and technology. The basic technological motivation is that smaller components should be faster and may also dissipate less heat. The most immediately apparent of the quantum dots properties is the emission of photons under excitation, which are visible to the human eye as light. Moreover, the wavelength of these photon emissions depends on quantum dot's size. On one hand, these systems are thought to have vast potential for future technological applications, such as possible applications in memory chips (C. Lee, 2007), quantum computation (Loss, & DiVincenzo, 1998), quantum cryptography (Molotkov, & Nazin, 1996), in room-temperature quantum-dot lasers (Huffaker et. al., 1998), and so on. More about quantum dots is mentioned in chapter 2.

The field of nanostructure physics has been growing rapidly in recent years, and much theoretical insight has been gained hand in hand with progress in experimental techniques and more device-oriented applications. Experiments on quantum dots have been mainly focused on electron transport properties and optical properties (Räsänen, Ph.D. Thesis, 2004). A full understanding of the

many recent optical and transport measurements on quantum dots requires detailed knowledge of the energies of the N-electron dot. One of the popular and effective methods to deal with particles in semiconductor QDs is the numerical exact diagonalization (Harju et. al, 1998; Que, 1992). This method has an intrinsic limitation with respect to the number of particles because of the rapidly growing dimension of matrices under diagonalization and is practically applicable to a QD with around ten electrons (P. A. Maksym, 2005). Apart from the computationally intensive approach of direct numerical diagonalization, the N-electron quantum dot system has been studied extensively by the Hartree approximation (Johnson, & Reina, 1992) as well as QMC methods (Bolton 1996; Harju, Svedlov, & Nieminen, 1998; Helle, 2006).

In electronic structure calculations the treatment of electron-electron interactions is the main source of difficulty. These interactions cannot easily be separated out or treated without approximation. Since Quantum Monte Carlo (QMC) methods treat electron-electron interactions almost without approximation, have become increasingly important tools to study correlated many-body systems (Foulkes et. al., 2001). The accuracy of QMC methods enables a great deal of confidence to be placed in the results obtained in various studies (Førre et.al., 2006; Harju, Sverdlov, & Nieminen, 1998; Pederiva, Umrigar, & Lipparini, 2000; Tsuchiya, 2004).

The VMC method forms the basics of the QMC machinery that provides a powerful tool for incorporating correlation effects into the many-body wave function, and by means of Monte Carlo integration the expectation values of different physical observables can be obtained. In the VMC approach *any* trial wave function may be optimized with respect to either the energy or the variance minimization. This method therefore allows flexibility beyond the orbital representation. In practice, however, the VMC method requires a trial wave function, that accurately represents the basic features of the eigenfunction, as

input. The accuracy of VMC is limited only by this function. Furthermore, accurate results are obtained for several systems (Harju, 2005; Saarikoski et. al., 2002).

A completely different and particularly interesting approach to the many-body problems is realized by combining MC integration with the effective Exact Diagonalization (ED) method. Commonly known as Monte Carlo Diagonalization (MCD) method, provides a highly efficient tool for solving quantum mechanical problems with many particles (Siljamäki et. al., 2005).

In this study the ground state energies of interacting two electron and electron-hole pair (exciton) in two dimensional disc-like as well as three dimensional spherical parabolic quantum dots are described by applying both the Variational Monte Carlo (VMC) and Monte Carlo Diagonalization (MCD) approaches and in some cases the results will be compared to the other studies. In addition, the effects of both dimensionality and confinement strength on exciton binding energies are also analyzed. The aim of this thesis is to describe and test new variational wave functions which permit easier and accurate evaluation of the ground-state energies of the interacting two particle in quantum dot systems. The general form of the trial variational wave functions is the harmonic-oscillator basis multiplied by different correlation forms. The main difference of this work, comparing to the previous similar studies, is correlation function constructed as common Jastrow factor multiplied by serial expansion in terms of Hylleraas-like coordinates. Although the integrals including Jastrow factor can not be evaluated analytically, Monte Carlo approaches lead to efficient and accurate results. Very few terms are needed to reach an accuracy comparable to more common wave function forms with large basis sets. The calculations are performed in the real-space, which gives the advantage to shape the external potential arbitrarily. This feature is essential when modelling the systems of the present work.

The results show that the Monte Carlo technique via the proposed ansatz is successfully implemented by computational code developed in this thesis. The technique used here with no constraints on the potential can be systematically improved by adding more terms using the procedure we described. The numerical code can be also optimized and parallelized for future applications on many particle systems.

The organization of this thesis is as follows. Before formulating the VMC and MCD algorithms several fundamental concepts with respect to Monte Carlo methods should be understood. We described these properties which form the basis of the work in chapter 3. QMC calculations crucially depend on the quality of the trial-function, and so it is essential to have an optimized wave-function as close as possible to the ground state. The problem of the function optimization is a very important topic in numerical simulation. We present some required features of trial wave functions and summarize the most common and efficient forms for different systems reported in literature in chapter 4. Four variational trial wave functions, established as the harmonic-oscillator basis multiplied by different correlation forms, are implemented in the calculations. Step by step improvement of trial wave functions are also outlined.

Two numerical approaches implemented in this thesis, VMC and MCD, are studied in chapter 5. A detail description of the program codes developed through the thesis has been omitted. Instead we focus on the theoretical principles regarding the numerical implementation.

In chapter 6 the interacting two particle problems are formulated, and then approximated to the forms suited for numerical calculations. The analytical solution to the one-electron quantum dot in a magnetic field is also presented. The presentation and discussion of the results are drawn and compared to other calculations in chapter 6.

Finally, the insights gained through the development of this thesis are presented in chapter 7, together with suggestions of further development of the numerical approaches.

CHAPTER TWO
QUANTUM DOTS

Quantum effects arise in systems which confine electrons to regions comparable to their de Broglie wavelength. When such confinement occurs in one dimension only, with free motion in the other directions, the so-called two dimensional (2D) systems which include thin films, layer structures, and quantum wells and superlattices are created. Confinement in two directions, with free motion in only one dimension gives the one-dimensional (1D) systems such as those solids in which linear chain-like structures can be identified, and semiconductor wires. The confinement on all three dimensions creates zero-dimensional (0D) systems such as clusters, quantum dots and colloids.

In recent years physicists and chemists have devoted increasing attentions to these materials systems, and the interest is expected to rise further in the near future, for reasons that low dimensional systems exhibits novel electronic and optical properties. Many differences between the electronic behaviors of bulk and quantum confined low-dimensional semiconductors are due to their different density of states. Figure 2.1 illustrates the different systems in a general way, and Figure 2.2 shows how the expected density of states varies with dimensionality. Passing from three dimensions to two dimensions the density N(E) of states changes from a continuous dependence N(E) $\propto E^{1/2}$ to a step-like dependence. Being zero dimensional, quantum dots have a sharper density of states than higher-dimensional structures. As a result, they have superior transport and optical properties, and are being researched for many technological applications listed briefly in subsection 2.4.

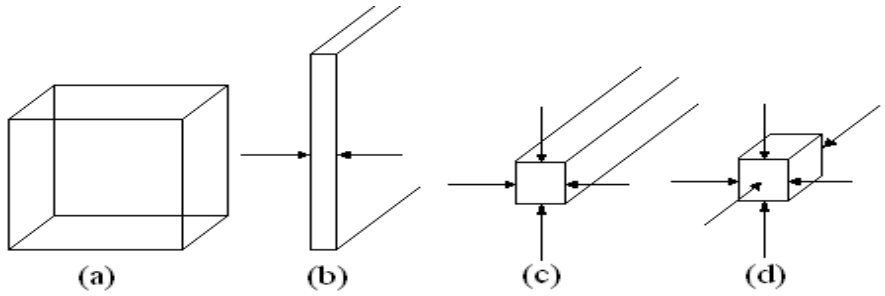

Figure 2.1 (a) bulk semiconductors, 3D; (b) thin films, layer structures, quantum wires, 2D; (c) linear chain structures, quantum wires, 1D; (d) clusters, colloids, microcrystallites, quantum dots, 0D.

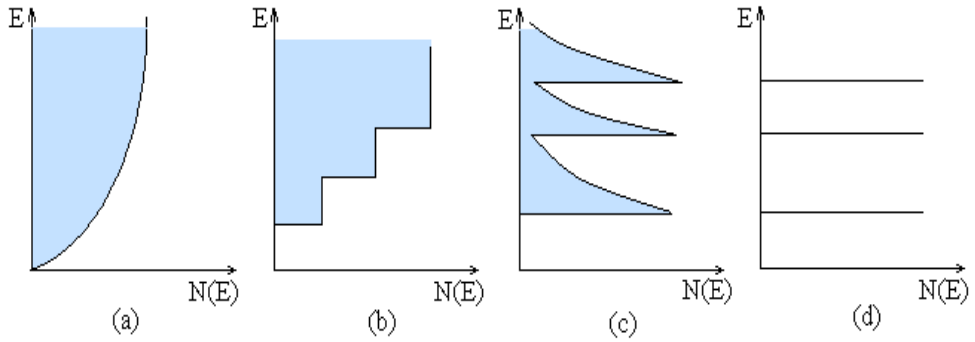

Figure 2.2 Densities of states N(E) for (a) 3D, (b) 2D, (c) 1D and (d) 0D systems (corresponding to ideal cases).

2.1 Historical Development

Engineering of less than three-dimensional semiconductors began in earnest during the early 1970s, when groups at AT&T Bell Laboratories and IBM made the first two-dimensional quantum wells. These structures, made by thin-film epitaxial techniques that build up a semiconductor one atomic layer at a time, are thin regions of semiconducting material (usually gallium arsenide and related compounds) that attract electrons. Quantum wells have now become commonplace. They are the basis of the laser diodes found in compact-disc

players and the sensitive microwave receivers that pull in signals from a satellite dish (M. A. Reed, 1993). In the meantime, researchers have learned how to confine electrons not simply in a plane but in a point.

The first hints that zero-dimensional quantum confinement was possible came in the early 1980s, when A. I. Ekimov and his colleagues at the Ioffe Physical-Technical Institute in St. Petersburg noticed unusual optical spectra from samples of glass containing the semiconductors cadmium sulfide or cadmium selenide (See Figure 2.5). The samples had been subjected to high temperature; Ekimov suggested tentatively that the heating had caused nanocrystallites of the semiconductor to precipitate in the glass and that quantum confinement of electrons in these crystallites caused the unusual optical behavior. Ekimov's hypothesis turned out to be true, but it took years of work by groups at Corning Glass, IBM, City College of New York and elsewhere to sort out the correct glass preparation techniques and convincingly demonstrate quantum confinement. Meanwhile Louis E. Brus and his co-workers at Bell Labs managed to synthesize colloidal nanocrystallites (Reed, 1993). All subsequent improved treatments in many laboratories world-wide follow on from their efforts. The developments in nanostructure experimental techniques and the unusual electronic and nonlinear optical properties of quantum dots led to sharp increase of number of publications on these systems per year. Figure 2.3 shows that since the first studies in the late eighties, the physics of quantum dots has been a very active and fruitful research topic.

2.2 Quantum Dots as artificial atoms

The term "Quantum Dot" was coined by Mark Reed and suggests an exceedingly small region of space. However, a semiconductor quantum dot is made out of roughly a million atoms with an equivalent number of electrons.

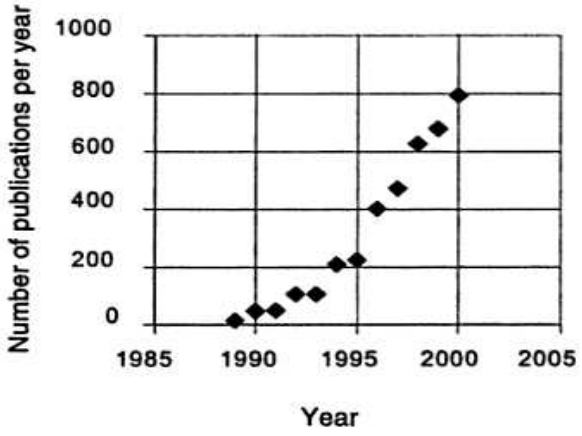

Figure 2.3 Increase of publications on quantum dots. Taken from Borovitskaya, & Shur (2002).

Virtually all electrons are tightly bound to the nuclei of the material, however, and the number of free electrons in the dot can be very small; between one and a few hundred. The de Broglie wavelength of these electrons is comparable to the size of the dot, and the electrons occupy discrete quantum levels (akin to atomic orbitals in atoms) and have a discrete excitation spectrum. This can be contrasted to quantum wires, which are confined to a line and quantum wells, which are confined to a planar region. Because of the analogies to real atoms, quantum dots are sometimes referred to as "artificial atoms". And rather than having to study different elements or isotopes, these effects can be investigated in a quantum dot by simply changing its size or shape. Their typical dimensions range from nanometers to a few microns, and their size, shape and interactions can be precisely controlled through the use of advanced nanofabrication technology. At 10 nanometers in diameter, nearly 3 million quantum dots could be lined up end to end and fit within the width of your thumb.

However unlike their naturally occurring brethren, artificial atoms can be

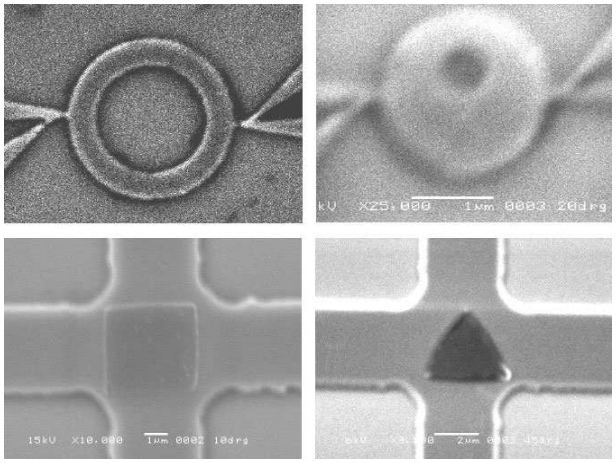

Figure 2.4 SEM micrographs of quantum dots with circular, asymmetric circular, square and triangular geometry. Taken from Morelle, Bekaert, & Moshchalkov, (2004).

manufactured in such a way to exhibit a precise control over this confinement, which has opened up a wide range of possibilities and areas for examination (Kouwenhoven et. al., 2001). There are several ways to confine excitons in semiconductors, resulting in different methods to produce quantum dots. For example, they are not limited to being spherically or circularly symmetric that we can have elliptic dots, rectangular dots, triangular dots, and even dots without any symmetry (Figure 2.4). The variety of different quantum-dot shapes is, however, continuously extending due to the rapid development of fabrication methods. The modeling of new nanoelectronic devices sets great demands on the computational tools, since the deviation from a circular geometry generally makes the many-electron problem particularly complicated to solve, especially in the presence of a magnetic field.

The confinement potential determines the electrostatic environment of the quantum dot and in general contains the information about the corresponding system. In a sense, the confinement potential provides a sensitive knob, which

can be tuned to control the electronic properties of the system. Because of this sensitivity, it is crucial to model the confinement potential as closely as possible to the experimental situation (A. Bychkov, 2003). The "hard wall" confining potential defined as:

$$V_{\text{ext}}(x,y) = \begin{cases} 0, \text{in the dot}, \\ \infty, \text{elsewhere}. \end{cases} \tag{2.2.1}$$

and usually lead to formation of circular quantum dots has been widely studied (Brunner et. al., 2004; Geerinckx et. al., 1990). Furthermore W. Xie (2003) reported calculations for two electron in a Gaussian confining potential quantum dot uder influence of a perpendicular homogeneous magnetic field.

Electrons in quantum dots are usually confined in an interface of a semiconductor heterostructure, e.g. GaAs/AlGaAs, so that the transverse dimensions, controlled by a lateral confinement, are considerably larger than the thickness of the dot. In modeling quantum dots, the most common approximation for the flat disk-like shape is a two-dimensional well with a parabolic confinement potential. In most cases this model describes the movement of the electrons with a reasonable accuracy. In this thesis we assumed parabolic confinement, usually known as "soft potential", for 2D as well as 3D GaAs quantum dot systems.

Experiments on quantum dots have been mainly focused on electron transport properties and optical properties (Räsänen, Ph.D. Thesis, 2004). The artificial atoms have universal spectral and transport properties that are independent of material, shape, or disorder. Electron transport is not studied in this thesis.

The optical properties of quantum dots are mainly related to the absorption or emission of light in the far-infrared (FIR) range, corresponding to the typical excitation energies in semiconductor quantum dots. Excitonic effects qualitatively alter the optical properties of reduced dimensional systems. The excited-state properties are of critical importance in device miniaturization and the design of

potential devices in many fields such as optoelectronics, photovoltaic cells and so on.

Excitons in QDs

In quantum dots, binding energies of excitons and excitonic complexes, such as trions and biexcitons, are much larger than those in the bulk materials, and these excitonic complexes strongly influence optical properties of quantum dots. In addition to interest of basic physics, these studies are driven by the need for a deep understanding of such confined states for the successful application of quantum structures to quantum information technologies. Large binding energy of the biexciton state is particularly important in light of the recent demonstration of the ability to operate a two-qubit gate using exciton and biexciton states.

Experimental evidence for quantum size effects of excitons confined in all three dimensions was obtained by Ekimov & Onuschenko (1981) for microcrystallites of CuCl dispersed in a silicate glass. They found a blue shift of the main excitonic absorption feature, and this is evident in Figure 2.5, taken from Yoffe (1993). This work lead directly to a theoretical treatment of this topic by Efros & Efros (1982), and it is the case that all subsequent improved treatments follow on from their efforts. Efros & Efros (1982) assumed spherical microcrystallites with infinite potential barriers at the crystallite boundary. They also applied the effective-mass approximation (EMA) and assumed parabolic energy bands. Denoting the average dot radius R and effective Bohr radius $a_B^* = \dfrac{4\pi\hbar^2\varepsilon}{\mu e^2}$, ($\mu = m_e^* m_h^*/(m_e^* + m_h^*)$ is reduced mass of electron-hole pair and ε is background dielectric constant of the semiconductor material) according to Kayanuma's report (Kayanuma, 1988) the motional state of the exciton is classified into three regimes:

1. $R/a_B^* \gtrsim 4$: This is the regime of weak confinement and the dominant energy is the Coulomb term, and there occurs a size quantization of the motion of

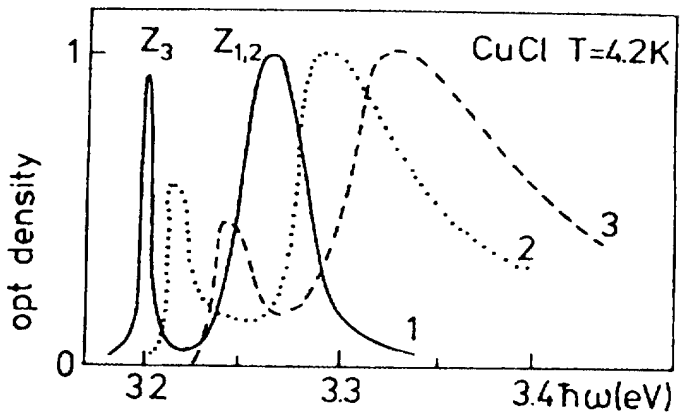

Figure 2.5 Shift in position of exciton peaks for CuCl microcrystallites as the radius R changes from 310$\mathring{A}$ (curve 1) to 29$\mathring{A}$ (curve 2) to 20$\mathring{A}$ (curve 3)(Taken from Yoffe, 1993).

exciton. Experimentally, semiconductors such as CuCl with $a_{\mathrm{B}} \approx 7\mathring{A}$, are suitable for study in this case.

2. The second case to consider is $R/a_B^* \lesssim 2$ and this is the regime of strong confinement. The Coulomb term now turns out to be small and can be ignored or treated as perturbation. The electrons and holes can be thought of as confined independent particles, so excitons are not formed, and separate size quantization of the electron and hole is the dominant factor. The electrons and holes are treated as independent particles, and for excited states we refer to electron-hole pairs rather than excitons. Suitable materials for investigations in this regime are the II-VI semiconductors, and also GaAs and Ge, for which a_{B} is relatively large.

3. The third case is for the condition $2 \lesssim R/a_B^* \lesssim 4$, and this is the intermediate regime. It is the electron motion which is now quantized and the hole interacts with it through the Coulomb potential.

For the experimentalist the important factor to consider first of all is the

magnitude of the bulk exciton binding energy and Bohr radius. For solids such as CuCl, $a_{\rm B}^* \approx 7.5\mathring{A}$ while, for CdSe, $a_{\rm B}^* \approx 54\mathring{A}$. It is therefore not surprising to find that experiments involved CuCl have been for the case when $R > a_{\rm B}^*$, while CdSe is suitable when $R < a_{\rm B}^*$.

Exciton binding energies E_b are larger than for bulk semiconductors. This means that, with the larger binding energy, 2D excitons in quantum wells such as GaAs and the wider-bandgap II-VI semiconductors are more stable than in the bulk crystals, and optical properties can be dominated by exciton effects even at room temperature, as found for example by Greene & Bajaj (1983) in their work on GaAs, by Pozina et.al. (1992) in their study of CdTe, and by Doran et. al. (1992) who investigated $Cd_{0.33}Zn_{0.67}Te$.

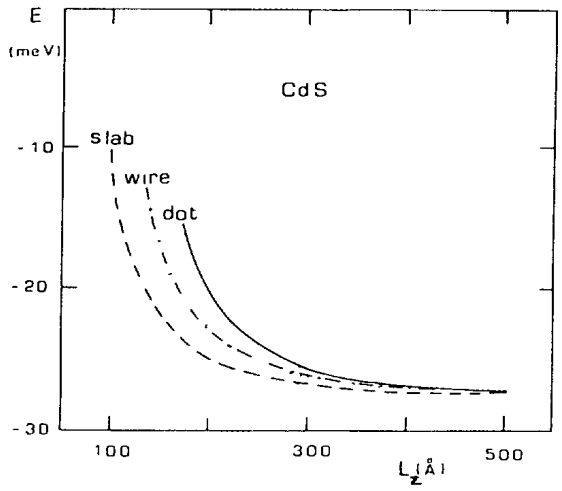

Figure 2.6 Exciton energies for cubic CdS in the form of a slab, wire and quantum dot of side L_z. Taken from Ref. Yoffe (1993).

To give reader some idea of how exciton binding energy vary with sample size for a slab (two dimensions), wire (one dimension) and quantum dot (zero dimension), Figure 2.6 gives energies for CdS in the cubic modification, as calculated by D'Andrea et. al. (1990). The ground-state exciton binding

energy E_{b} for the bulk crystal was taken as 28 meV, M = $0.94\mathrm{m}_0$, $\varepsilon = 8.1$. For the slab, L_z is the thickness; for the wire, $L_x = L_y = L$; for the quantum dot, $L_x = L_y = L_z = L$ with $L > 3a_{\mathrm{B}}$.

2.3 Fabrication of QDs

Semiconductor quantum dots are fabricated with several different methods. The common objective between the techniques is to produce a lateral confinement of the two-dimensional electron gas (2DEG) at the interface between two semiconducting materials. One of the earliest methods was to create metal electrodes on the heterostructure surface with lithographic techniques. A voltage applied to the electrodes confines the 2DEG existing at the interface between the layers of different materials, e.g., GaAs and AlGaAs, into a small area. The density of the 2DEG can be controlled by the gate voltage applied to the conductive substrate. The benefit of the method is the absence of edge defects, characteristic of etched quantum dots. A serial structure of lateral quantum dots may also be suitable for quantum computation, since all the tunnel barriers can be freely controlled. This would require the isolation of a single electron (Räsänen, Ph.D. Thesis, 2004). Individual quantum dots can be created by a technique called electron beam lithography, in which a pattern is etched onto a semiconductor chip, and conducting metal is then deposited onto the pattern.

Reed and co-workers performed the pioneering experiments in creating vertical quantum-dot systems by etching techniques (Reed, 1993). By inserting electric contacts on the both ends of the heterostructure pillars and measuring electronic transport through the device, they could observe a discrete spectrum of quantum states. Later, Tarucha et al. (1996) managed to measure Coulomb oscillations in vertical quantum dots containing a controlled number of electrons, and a clear shell structure was revealed. The dot is formed between nonconducting barrier

layers, separating it from the source and drain contacts, and the lateral potential is tuned by a negative voltage applied to a metal gate around the pillar. In comparison with lateral quantum dots, the number of electrons is generally easier to control in the vertical transport. Etching techniques also enable the shaping of the quantum-dot geometry.

Quantum dots can also be fabricated using a growth mechanism of a semiconducting compound on the surface of a material with a wider band gap than the growing material. The growth can be selective or self-assembled, depending on the material parameters. In the latter case, a sufficient difference in the lattice constants between the compounds, e.g. GaAs and InAs, is required to induce the growth of quantum-dot structures. Self-assembled quantum dots are considerably smaller and more strongly confined than their lithographically fabricated counterparts (Poole, & Owens, 2003). Hence, their energy-quantization regime is suitable for developing optical devices, e.g., quantum-dot lasers. Highly ordered arrays of quantum dots may also be self assembled by electrochemical techniques. A template is created by causing an ionic reaction at an electrolyte-metal interface which results in the spontaneous assembly of nanostructures, including quantum dots, on the metal which is then used as a mask for mesa-etching these nanostructures on a chosen substrate. Yet another method is pyrolytic synthesis, which produces large numbers of quantum dots that self-assemble into preferential crystal sizes.

In semiconductors, quantum dots are small regions of one material buried in another with a larger band gap. Quantum dots sometimes occur spontaneously in quantum well structures due to monolayer fluctuations in the well's thickness. Self-assembled quantum dots nucleate spontaneously under certain conditions during molecular beam epitaxy (MBE) and metallorganic vapor phase epitaxy (MOVPE), when a material is grown on a substrate to which it is not lattice matched. The resulting strain produces coherently strained

islands on top of a two-dimensional "wetting-layer". This growth mode is known as Stranski-Krastanov growth. The islands can be subsequently buried to form the quantum dot (Knuuttila, Ph.D. Thesis, 2006). This fabrication method has the most potential for applications in quantum cryptography (i.e. single photon sources) and quantum computation. The main limitations of this method are the cost of fabrication and the lack of control over positioning of individual dots.

In large numbers, quantum dots may also be synthesized by means of a colloidal synthesis. Epitaxy, lithography, and colloidal synthesis all have different positive and negative aspects. By far the cheapest, colloidal synthesis also has the advantage of being able to occur at benchtop conditions and is acknowledged to be the least toxic of all the different forms of synthesis.

Quantum dots can be made from a range of materials, currently the most commonly used materials include zinc sulphide, lead sulphide, cadmium selenide and indium phosphide. Many of the promising applications for quantum dots will see them used within the human body. In order to avoid toxic materials leaching from the quantum dots, they are also coating in a protective polymer (Stream Chemicals, Inc., 2006).

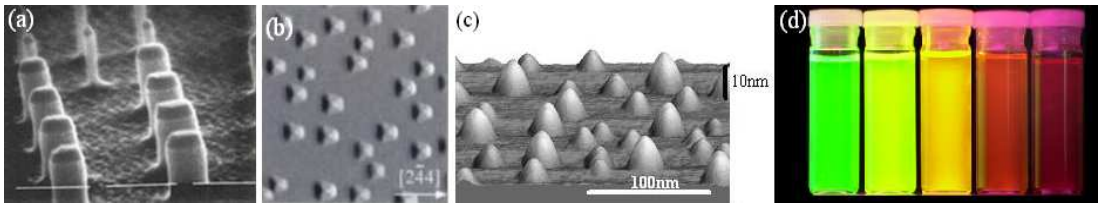

Figure 2.7 (a) Litographic quantum dots, (b) AFM image of MOVPE-grown $In_{0.35}Ga_{0.65}As$ QD grown on (411)B substrate at 650^{o}C (Taken from Ref. Masumoto & Takagahara, 2002), (c)AFM image of InAs epitaxical island quantum dots grown on GaAs substrate (Taken from Nanostructure Materials & Devices Laboratory web page, University of Southern California), (d) colloidal quantum dots.

2.4 Applications

Nearly 20 years after their discovery, semiconductor quantum dots are emerging as a bona fide industry with a few start-up companies poised to introduce products this year. Initially targeted at biotechnology applications, such as biological reagents and cellular imaging, quantum dots are being eyed by producers for eventual use in light-emitting diodes (LEDs), lasers, and telecommunication devices such as optical amplifiers and waveguides. The strong commercial interest has renewed fundamental research and directed it to achieving better control of quantumdot self-assembly in hopes of one day using these unique materials for quantum computing (Ouellette, 2003). By applying small voltages to the leads, one can control the flow of electrons through the quantum dot and thereby make precise measurements of the spin and other properties therein. With several entangled quantum dots, or qubits, plus a way of performing operations, quantum calculations might be possible.

Quantum dots have quickly found their way into homes in many electronics. The new PlayStation 3 and DVD players to come out all use a blue laser for data reading. The blue laser up until only a few years ago was beginning to be seen as something of an impossibility, until the synthesis of a blue quantum dot laser (Nanofm Ltd., n.d.).

In modern biological analysis, various kinds of organic dyes are used. However, with each passing year, more flexibility is being required of these dyes, and the traditional dyes are simply unable to meet the necessary standards at times. To this end, quantum dots have quickly filled in the role, being found to be superior to traditional organic dyes on several counts, one of the most immediately obvious being brightness (owing to the high quantum yield) as well as their stability. Currently under research as well is tuning of the toxicity. (Deak Lam Ltd., n.d.)

In the case of colloids, the microcrystallites are normally present as suspensions in liquids, or disturbed in a glass or rocksalt matrix which have large optical energy gaps. For example colloidal particles of semiconductors such as CdS or CdSe dispersed in glass are well known and widely used as optical cut-off color filters for the visible part of the optical spectrum, and also in stained-glass windows (Yoffe, 1993).

CHAPTER THREE
FUNDAMENTALS OF MONTE CARLO METHODS

3.1 Introduction to Monte Carlo Methods

The numerical methods that are known as Monte Carlo methods can be loosely described as statistical simulation methods, where statistical simulation is defined in quite general terms to be any method that utilizes sequences of random numbers to perform the simulation. Monte Carlo methods have been used for centuries, but only in the past several decades has the technique gained the status of a full-fledged numerical method capable of addressing the most complex applications. The name "Monte Carlo" was coined by Metropolis (inspired by Ulam's interest in poker) during the Manhattan Project of World War II, because of the similarity of statistical simulation to games of chance, and because the capital of Monaco was a center for gambling and similar pursuits. Monte Carlo is now used routinely in many diverse fields, from the simulation of complex physical phenomena such as radiation transport in the earth's atmosphere and the simulation of the esoteric subnuclear processes in high energy physics experiments, to the mundane, such as the simulation of a Bingo game. The analogy of Monte Carlo methods to games of chance is a good one, but the "game" is a physical system, and the outcome of the game is not a pot of money or stack of chips (unless simulated) but rather a solution to some problem. The "winner" is the scientist, who judges the value of his results on their intrinsic worth, rather than the extrinsic worth of his holdings (Drakos, 1995).

Monte Carlo Methods are a class of techniques that can be used to simulate the behavior of a physical or mathematical system. They are distinguished from other simulation methods such as molecular dynamics, by being *stochastic*, that is, *non-deterministic* in some manner. This stochastic behavior in Monte Carlo

Methods generally results from the use of random number sequences. Although it might not be surprising that such an analysis can be used to model random processes, Monte Carlo methods are capable of much more. A classic use is for the evaluation of definite integrals, particularly multidimensional integrals with complicated boundary conditions. The use to which we will apply Monte Carlo is the solution of the well-known partial differential equation, the Schrödinger equation.

Monte Carlo methods are frequently applied in the study of systems with a large number of strongly coupled degrees of freedom. Examples includes liquids, disordered materials, and strongly coupled solids. Unlike ideal gases or perfectly ordered crystals, these systems do not simplify readily. The many degrees of freedom present are not separable, making a simulation method, such molecular dynamics or Monte Carlo, a wise choice. Furthermore, use of Monte Carlo is advantageous for evaluating high dimensional integrals, where grid methods become inefficient due to the rapid increase of the number of grid points with dimensionality. Monte Carlo also can be used to simulate many classes of equations that are difficult to solve by standart analytical and numerical methods.

Statistical simulation methods may be contrasted to conventional numerical discretization methods, which typically are applied to ordinary or partial differential equations that describe some underlying physical or mathematical system. In many applications of Monte Carlo, the physical process is simulated directly, and there is no need to even write down the differential equations that describe the behavior of the system. The only requirement is that the physical (or mathematical) system be described by probability density functions (pdf's), which will be discussed in more detail later in this chapter. For now, we will assume that the behavior of a system can be described by pdf's. Once the pdf's are known, the Monte Carlo simulation can proceed by random sampling from the pdf's. Many simulations are then performed

(multiple "trials" or "histories") and the desired result is taken as an average over the number of observations (which may be a single observation or perhaps millions of observations). In many practical applications, one can predict the statistical error (the "variance") in this average result, and hence an estimate of the number of Monte Carlo trials that are needed to achieve a given error.

Given our definition of Monte Carlo, let us now describe briefly the major components of a Monte Carlo method. These components comprise the foundation of most Monte Carlo applications, and the following sections will explore them in more detail. An understanding of these major components will provide a sound foundation for the reader to construct his or her own Monte Carlo method, although of course the physics and mathematics of the specific application are well beyond the scope of this chapter. The primary components of a Monte Carlo simulation method include the following:

- *Probability distribution functions* (pdf's) - the physical (or mathematical) system must be described by a set of pdf's.
- *Random number generator* - a source of random numbers uniformly distributed on the unit interval must be available.
- *Sampling rule* - a prescription for sampling from the specified pdf's, assuming the availability of random numbers on the unit interval, must be given.
- *Scoring (or tallying)* - the outcomes must be accumulated into overall tallies or scores for the quantities of interest.
- *Error estimation* - an estimate of the statistical error (variance) as a function of the number of trials and other quantities must be determined.
- *Variance reduction techniques* - methods for reducing the variance in the

estimated solution to reduce the computational time for Monte Carlo simulation.

- *Parallelization and vectorization* - algorithms to allow Monte Carlo methods to be implemented efficiently on advanced computer architectures.

The remainder of this chapter will describe only those concepts needed later in this thesis. Further details may be found in standart statistics texts (see Hammond, Lester, & Reynolds, 1994).

3.2 Scaling of Computer Time

To see the advantage of Monte Carlo methods over fixed grid methods for high dimensional integrals we need to compare the error of each method for different numbers of dimensions.

Imagine that the total number of function evaluations for a program run is n and the number of dimensions is d. We perform the integration over a fixed region of high dimensional space Ω.

If the estimate of the integral is obtained using Simpson's rule, the integrand is evaluated in n hypercubes of volume h^d, where h is the width of a "strip" in the fixed grid scheme. Hence, we have that

$$\Omega = nh^d \quad \text{and} \quad h = \left(\frac{\Omega}{n}\right)^{\frac{1}{d}} \sim n^{-\frac{1}{d}} \tag{3.2.1}$$

The proportional error in the integral per unit cell is approximately h^4 which becomes

$$\left(\frac{\Omega}{n}\right)^{\frac{4}{d}} \sim n^{-\frac{4}{d}} \tag{3.2.2}$$

Hence the proportional error decreases like $n^{-\frac{4}{d}}$ as the number of function evaluations, n, increases.

The error in the Monte Carlo method is independent of the number of dimensions and is simply proportional to $1/\sqrt{n}$. Comparing these errors for different d values in Figure 3.1, we see that for $d > 8$ the errors in the Monte Carlo estimate decrease more quickly as n increases. We see that for a higher number of dimensions, MC methods give greater accuracy (James, Ph.D. Thesis, 1995).

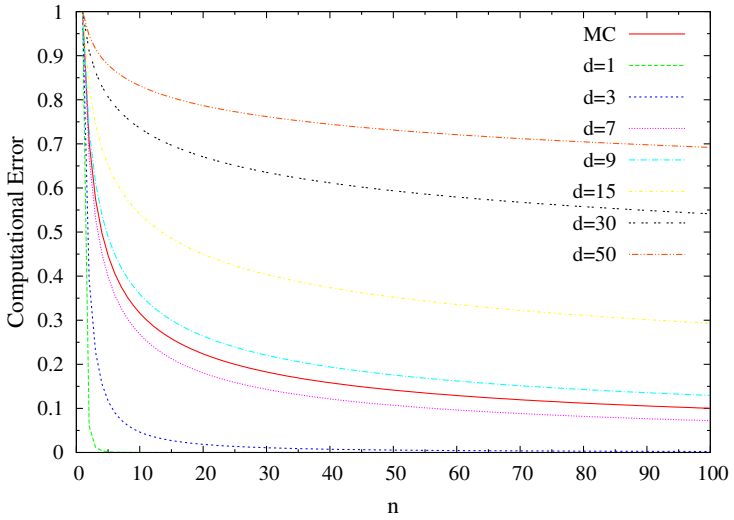

Figure 3.1 Comparing the accuracy of MC and Simpson's rule for differing dimensions in the integral.

3.3 Random Numbers Analysis

God not only play dice. He also sometimes throws the dice where they can not be seen.

Stephen Hawking

Monte Carlo simulation has become one of the most important tools in all fields of science. Monte-Carlo simulation consists of repeating the same basic calculation a large number of times with different input data and then performing some statistical analysis on the set of results. Input data for the different "trials" are selected using values in prescribed distributions, using a pseudo-random number generator. The basic computation typically involves a significant amount of calculation, so that the pseudo-random number generation itself represents a small fraction of the total computational effort. The success of any Monte Carlo application depends crucially on the quality of the pseudo-random number generators used. To achieve the theoretical convergence rates associated with the method, the pseudo-random number generators must have certain properties. Both the quality of the generators and the statistical independence of the results calculated on each MC step are important (Wikramaratna, 2000). A loose definition of random number is a numerical value resulting from a process or experiment whose value cannot be predetermined by the initial conditions. It is important to note that the term "random number" is somewhat misleading; a number is not random, rather it is the relationship between numbers in a set which is random. The result of an inherently random physical process, such as the decay of radioactive nuclei or the decay of subatomic particles to the trajectories of dust particles across the surface of a liquid, yields *truly* random results. Computers, on the other hand, are precise and deterministic; therefore, "random" numbers generated by computers are often called pseudo-random numbers. This happens to be significantly more difficult on a computer than one might initially expect. Unfortunately, there is no consensus on the best way of obtaining such random numbers. Moreover, there is not a consistent set of requirements or terminology between different solutions (Viega, 2003). Pseudo-random numbers are generated by deterministic computational processes, but the numbers satisfy one or more statistical tests for randomness. The more statistical tests for randomness a sequence of pseudo-random numbers passes, the higher the

quality of the pseudo-random numbers. Details of these tests will not be covered here but can be found in elsewhere (see Hammond, Lester, & Reynolds, 1994). Methods for producing pseudorandom numbers and transforming those numbers to simulate samples from various distributions are among the most important topics in statistical computing. For many problems, high-quality pseudo-random numbers are overkill, but, for other problems, high-quality pseudo-random numbers are critical to obtaining the correct results for a calculation.

Many types of numerical simulations, including Quantum Monte Carlo, require the generation of random numbers with respect to a given probability density function. Virtually all schemes to generate random numbers with respect to a given probability density function rely on uniform random numbers. Uniform random numbers are random numbers that fall between 0 and 1, with all numbers having an equal probability of being generated.

This thesis covers basic principles of random numbers in Monte Carlo simulation. Current techniques or search for newer methods for random number generation is out of scope of the thesis.

A linear congruential generator (LCG) represents one of the oldest and best-known pseudorandom number generator algorithms. The theory behind them is easy to understand, and they are easily implemented and fast. A sequence $\{I_i\}$ of nonnegative integers is generated by means of the fundamental congruence relationship

$$I_{i+1} = aI_i + c \pmod{m} \tag{3.3.1}$$

where the multiplier a, the increment c, and the modulus m are nonnegative integers. From Equation 3.3.1, it is easy to show that $I_i < m$ for all i. Because of this, the sequence $\{I_i\}$ contains at most m distinct numbers. Using this result,

a set of uniform pseudo-random numbers, $\{U_i\}$, can be obtained by letting

$$U_i = \frac{I_i}{m} \tag{3.3.2}$$

Because Equation 3.3.1 is deterministic and because I_i is bounded, the sequence $\{I_i\}$ is composed of repeating subsequences. The period of the sequence $\{I_i\}$, p, is equal to the length of the repeating subsequence. As an example, consider the case where $a = c = I_0 = 3$ and $m = 5$. Here the generator, $I_{i+1} = 3I_i + 3 \pmod 5$, produces the sequence $\{3, 2, 4, 0, 3, 2, 4, \ldots\}$. This sequence is composed of repetitions of the subsequence $\{3, 2, 4, 0\}$ and has a period of $p = 4$.

Obviously when generating pseudo-random numbers, a and c should be chosen so that the sequence $\{I_i\}$ has a maximum period ($p = m$). This ensures that the uniform pseudo-random number generator produces the maximum number of distinct pseudorandom numbers. This full period occurs if and only if:

1. c is relatively prime to m (or equivalently gcd $(c, m) = 1$).
2. $a \equiv 1 \pmod g$ for every prime factor g of m.
3. $a \equiv 1 \pmod 4$ if m is a multiple of 4.

Because current computers use binary numbers, the most efficient LCGs have an m equal to a power of 2, most often $m = 2^{32}$ or $m = 2^{64}$, because this allows the modulus operation to be computed by merely truncating all but the rightmost 32 or 64 bits. Poor choices had led to ineffective implementations of LCGs. The following table lists the parameters of LCGs in common use:

The quality of sequences generated using linear congruential generators is determined by the period length and the results of standard statistical tests for pseudorandom numbers.

Table 3.1 The parameters of linear congruential generators used by common libraries.

Source	m	a	c
Numerical Recipies	2^{32}	1664525	1013904223
glibc (Used by GCC)	2^{32}	1103515245	12345
Microsoft Visual/Quick C/ C++	2^{32}	214013	2531011

In this thesis we use the linear congruential generator of Intel Fortran compiler 10.0 for Linux, seeded with a character generated from system clock (see the algorithm below). It is extremely simple to code and can be implemented in virtually any high-level programming language. It can be coded as a subroutine or function, or, for maximum computational efficiency, we coded in-line.

Algorithm 1. Random number generator with seed from system clock.

```
INTEGER(I4B)::Count
INTEGER(I4B), DIMENSION(2) ::  Seed
CALL SYSTEM_CLOCK(Count)
Seed = Count
CALL RANDOM_SEED(PUT=Seed)
```

Modifications can be made to linear congruential generators to improve the algorithm's results in standard statistical tests. One such modification simply shuffles the sequence generated by a linear congruential generator.

In addition to linear congruential generators, uniform random numbers can be created using multiplicative congruential generators. These generators are the same as the linear version except $c = 0$. In this case, it is not possible to choose a

so that the sequence $\{I_i\}$ has a full period; however, to optimize the method, it is possible to choose a and I_0 so that the sequence has a maximum period. Because fewer operations are performed, multiplicative congruential generators are faster than linear congruential generators.

Monte-Carlo simulations are common and inherently well suited to parallel processing, thus requiring random numbers that are also generated in parallel. Generating parallel random numbers as well as parallelization of the current code are planed future works.

3.4 Probability Density and Distribution Functions

We need to start by defining the concepts and notation used to discuss random numbers and events. An *experiment* is the process of observing one or a set of physical properties in a system of interest. The result of an experiment is limited to certain values of ranges of values of the physical properties. A *state* is an allowed value of the set of physical properties of the system. The set of all possible states is the *sample space*. A *discrete* sample space contains either a finite or infinite number of distinct values. A *continuous* sample space contains an infinite numbers of continuous values (such as the positions of particles). A *sample point* is a single point in sample space. A *random variable* is a variable whose value lies within the sample space with a certain probability distribution. To avoid confusion, we will use upper case (X, Y, Z) to denote sample points and lower case (x, y, z) to denote variables. This distinction will become clear with usage. A *sequence* is a series, in order of occurrence, of sample points resulting from an experiment. We often will use the set notation $\{X_i\}$ to denote all the members of a sequence.

The most familiar uses of random numbers occur in games of chance. This

connection gives the Monte Carlo method its name. Consider a standart six-sided die. If one tosses an ideal,unbiased die, and records the outcome for a sufficiently large number of tosses (in principle, an infinite number), each of the six outcomes will occur exactly one sixth of the time. Even though the outcome of a single toss is random, and thus unknown beforehand, the probability of each outcome is 1/6. The *probability density function* is the function that describes the probabilities of all possible events. The sum or integral of the probabilities must be unity to insure the proper normalization of the density function. For a discrete distribution the normalized probability function p must satisfy,

$$\sum_{i=1}^{N} p(x_i) = 1, \tag{3.4.1}$$

where the sum is over all states, x_i. In the case of die, the normalized probability density function is $p(x_i) = 1/6$, for each $x_i = 1, 2, 3, 4, 5, 6$.

A continuous density function describes the probability of an event associated with a continuous variable. The *probability density function* represents the probability that the value of a given sample point is less than or equal to x, i.e.

$$P(x) = \int_{-\infty}^{x} p(y)dy \tag{3.4.2}$$

(We will use lower case to denote density functions and upper case to denote the associated distribution functions.) The distribution function always increases monotonically from zero to one. If $P(x)$ is defined as a probability density function, it must be positive for all random x variables:

$$P(x) > 0, \qquad -\infty < x < \infty \tag{3.4.3}$$

The probability of a random variable to occur on any point of the real axis is

unity:

$$\int_{-\infty}^{\infty} p(x')dx' = 1 \tag{3.4.4}$$

The probability of a random variable to be in the range of $(x, x + dx)$ is defined as:

$$P(x \leq x' \leq x + dx) = f(x)dx \tag{3.4.5}$$

Similarly the probability of the random variable to be in the finite range of [a,b] is given as:

$$P(a \leq x \leq b) = \int_a^b f(x')dx'. \tag{3.4.6}$$

Let us illustrate these concepts by examining two cases that will be of importance in MC simulations: the *uniform* and *Gaussian* distributions (see Figures 3.2 and 3.3). The density function of the uniform distribution is illustrated in Figure 3.2. For the uniform distribution, denoted by $u(x)$, all outcomes in a given range $[\alpha, \beta]$ have equal probability, and all other values of x have zero probability. The normalization of u requires that

$$u(x) = \begin{cases} (\beta - \alpha)^{-1} & \alpha \leq x \leq \beta, \\ 0 & \text{otherwise.} \end{cases} \tag{3.4.7}$$

If $u(x)$ is uniform probability distribution function, the probability of a random number to be between x and $x + dx$ is determined as:

$$u(x)dx = \begin{cases} dx & 0 < x < 1, \\ 0 & \text{otherwise.} \end{cases} \tag{3.4.8}$$

Therefore the probability that x is between a and b if $\alpha \leq a < b \leq \beta$ is given by

$$\int_a^b u(x)dx = U(b) - U(a) = (b - a)/(\beta - \alpha) \tag{3.4.9}$$

where U is the distribution function associated with u.

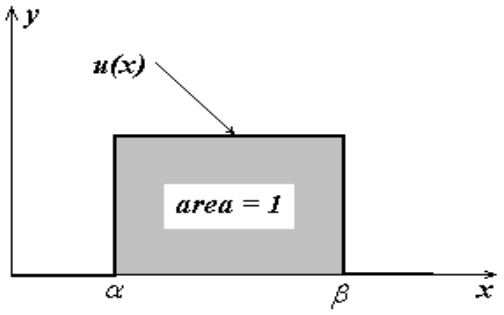

Figure 3.2 Uniform probability distribution function.

The Gaussian probability distribution function, $g(x)$, shown in Figure 3.3, owes much of its importance to the central limit theorem. In one dimension its density function is

$$g(x) = \frac{e^{-(x-\mu)^2/2\sigma^2}}{\sqrt{(2\pi\sigma^2)}}, \tag{3.4.10}$$

where the parameter μ specifies the center of the density function and σ determines its width.

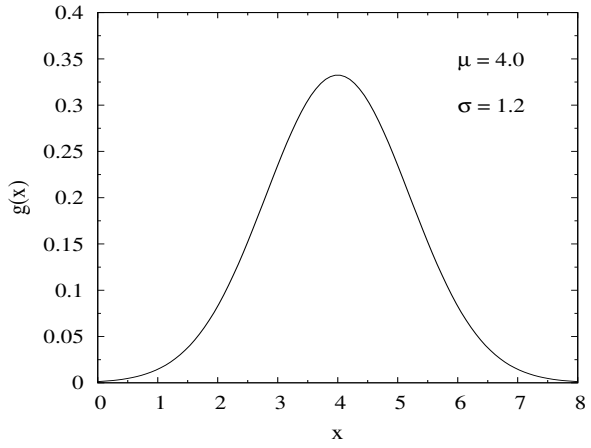

Figure 3.3 Gaussian probability distribution function.

3.5 Monte Carlo Integration

Monte Carlo methods are a way of using random numbers to perform numerical integrations. By way of example consider the integral

$$I = \int_{x_1}^{x_2} f(x)dx \tag{3.5.1}$$

There are many quadrature methods, with varying degrees of accuracy, which can be used to evaluate this integral. The trapezium and Simpson algorithms are both quadrature methods which involve evaluating $f(x)$ at evenly spaced points, x_i, on a grid. A weighted average of these values $f(x_i)$ gives an estimate of the integral

$$I_{\text{estimate}} = (x_2 - x_1)\frac{\sum_i \omega_i f(x_i)}{\sum_i \omega_i}, \tag{3.5.2}$$

where the ω_i are the weights. The weights and the sampling points are different for different methods of quadrature but all the methods sample the function $f(x)$ using pre-determined weights and sampling points.

Monte Carlo methods do not use specific sampling points but instead we choose points at random. The Monte Carlo estimate of the integral is then,

$$I_{\text{estimate}} = (x_2 - x_1)\frac{1}{N}\sum_{i=1} f(x_i) \tag{3.5.3}$$

$$= (x_2 - x_1)\overline{f}, \tag{3.5.4}$$

where the x_i are randomly sampled points and $\overline{f}$ is the arithmetic mean of the values of the function $f(x)$ at the sampling points. The standart deviation of the mean is given by

$$\sigma_m = \frac{\sigma}{\sqrt{N}}, \tag{3.5.5}$$

where

$$\sigma^2 = \frac{\sum_i (f(x_i) - \overline{f})^2}{N-1} \tag{3.5.6}$$

gives an estimate of the statistical error in the Monte Carlo estimate of the integral. Note that the error goes as $\frac{1}{\sqrt{N}}$, independent of the dimensionality of the integral.

3.5.1 Metropolis Sampling

The term "Monte Carlo" was first coined by Metropolis in 1947 in a paper on the diffusion of neutrons in fission-able material (Metropolis & Ulam, 1949). This was also the first paper to use the Metropolis algorithm, though many have used it since. The Metropolis algorithm is the most widely used algorithm for generating a sequence of phase space points that sample a given probability distribution. In quantum MC, each phase space point is a vector, $\mathbf{R} = \{\mathbf{r}_1, \mathbf{r}_2, ..., \mathbf{r}_{N-1}, \mathbf{r}_N\}$, in the $3N$ dimensional space of the position coordinates of all the N electrons, and the sequence phase space points provides a statistical representation of the ground state of the system.

If we are to build up a statistical picture of the overall system of electrons and nuclei, it is necessary to move the electrons around to cover all possible positions and hence all possible states of the system. As we move the electrons around, we can keep track of physical quantities such as the total energy, polarization, etc., associated with the *instantaneous* state of the electron configuration. The sequence of individual *samples* of these quantities can be combined to arrive at average values which describe the quantum mechanical state of the system. This is the fundamental idea behind the Monte Carlo method, and the Metropolis algorithm is used to generate the sequence of different states to sample physical quantities such as the total energy efficiently. Many pseudo-random numbers are used to generate the sequence of states, which are collectively called a *random*

walk.

The method described so far is rather simplistic. We have not decided on the probability distribution from which we shall draw the points, $\mathbf{R}$, to discussed how to sample the distribution once it has been chosen. We will return to the first question later, but let us ignore it for the time being and suppose only that we wish to sample some known distribution $\rho(\mathbf{R})$. Metropolis showed that the sampling is most easily accomplished if the points $\mathbf{R}$ form a Markov chain. There are two properties which must be satisfied if the random walk is the Markovian. These are:

1. Each point on the walk belongs to a finite set $\{\mathbf{R}_0, \mathbf{R}_1, ...\mathbf{R}_n, ...\}$ called a *phase space.*

2. The position of each point in the chain depends only on the position of the preceding point and lies close to it in the phase space.

Because of these properties, a Markov process may be completely specified by choosing values of the transition probabilities $P(\mathbf{R}_n, \mathbf{R}_m)$. Given that the walk has reached the point $\mathbf{R}_n$, $P(\mathbf{R}_n, \mathbf{R}_m)$ is the probability that the next point on the walk will be the point $\mathbf{R}_m$. The Metropolis algorithm works by choosing the transition probabilities in such a way that the points on the random walk sample the required probability distribution.

To understand the Metropolis algorithm, it is necessary to work out the statistical properties of the points on the Markov chain specified by the transition probabilities $P(\mathbf{R}_n, \mathbf{R}_m)$. This may be done by considering a very large ensemble of Markov chains, all evolving simultaneously according to the same transition probabilities. Making a physical analogy, we can imagine generating each Markov chain in the ensemble by moving a fictitious particle,

called a *walker*, around the phase space. The walkers all move step by step in accordance with the given transition probabilities, $P(\mathbf{R}_n, \mathbf{R}_m)$, and hence each walker generates one of the chains in the ensemble. At any given time, t, the number of walkers at point $\mathbf{R}_n$ is $N(\mathbf{R}_n, t)$. As the Markov chains evolve in time (the walkers move around), $N(\mathbf{R}_n, t)$, develops according to the Master equation,

$$\frac{d}{dN}N(\mathbf{R}_n, t) = -\sum_{\mathbf{R}_m} P(\mathbf{R}_n, \mathbf{R}_m)N(\mathbf{R}_n, t) + \sum_{\mathbf{R}_m} P(\mathbf{R}_m, \mathbf{R}_n)N(\mathbf{R}_m, t) \quad (3.5.7)$$

on the RHS is the total rate of transitions out of state $\mathbf{R}_n$ and the second is the total rate of transitions into the state $\mathbf{R}_n$. The change of walker density is zero in the long time limit, so that $N(\mathbf{R}_n, t) \to N(\mathbf{R}_n)$ as $t \to \infty$. The LHS of the Master equation becomes zero and $N(\mathbf{R}_n)$ satisfies

$$\sum_{\mathbf{R}_m} P(\mathbf{R}_n, \mathbf{R}_m)N(\mathbf{R}_n) = \sum_{\mathbf{R}_m} P(\mathbf{R}_m, \mathbf{R}_n)N(\mathbf{R}_m) \quad (3.5.8)$$

Metropolis realized that the distribution of walkers will settle down to the required distribution, $\rho(\mathbf{R})$, as long as the transition probabilities obey the *detailed balance* equation,

$$P(\mathbf{R}_n, \mathbf{R}_m)\rho(\mathbf{R}_n) = P(\mathbf{R}_m, \mathbf{R}_n)\rho(\mathbf{R}_m) \quad (3.5.9)$$

Imposing the condition of detailed balance on the transition probabilities gives the following equation,

$$\sum_{\mathbf{R}_m} P(\mathbf{R}_n, \mathbf{R}_m) \left(N(\mathbf{R}_n) - \frac{\rho(\mathbf{R}_n)}{\rho(\mathbf{R}_m)} N(\mathbf{R}_m) \right) = 0 \quad (3.5.10)$$

The solution to this steady state Master equation is

$$\frac{\rho(\mathbf{R}_n)}{\rho(\mathbf{R}_m)} = \frac{N(\mathbf{R}_n)}{N(\mathbf{R}_m)} \quad \text{for all pairs } \mathbf{R}_n \text{ and } \mathbf{R}_m \quad (3.5.11)$$

showing that $N(\mathbf{R}_n)$, the number of walkers in the state $\mathbf{R}_n$, becomes proportional to the steady state distribution, $\rho(\mathbf{R}_n)$, that we wish to sample.

We still have some freedom in choosing the transition probabilities, which are not uniquely defined by the detailed balance condition. In the Metropolis approach (Metropolis et. al., 1953) the walk is generated by starting from a point $\mathbf{R}_n$ and making a *trial move* to a new point $\mathbf{R}_m$ somewhere nearby in phase space. The rule for making trial moves is not crucial, expect that it is important to ensure that

$$P_{trial}(\mathbf{R}_n, \mathbf{R}_m) = P_{trial}(\mathbf{R}_m, \mathbf{R}_n) \tag{3.5.12}$$

Once the trial move has been made, it is *accepted* or *rejected* according to the rule

$$P_{accept}(\mathbf{R}_n, \mathbf{R}_m) = \min\left(1, \frac{\rho(\mathbf{R}_m)}{\rho(\mathbf{R}_n)}\right) \tag{3.5.13}$$

which is implemented as follows,

$$P_{accept}(\mathbf{R}_n, \mathbf{R}_m) = \begin{cases} 1 \quad i.e. \text{ always accept if } \frac{\rho(\mathbf{R}_m)}{\rho(\mathbf{R}_n)} \geq 1 \\ \frac{\rho(\mathbf{R}_m)}{\rho(\mathbf{R}_n)} \quad i.e. \text{ accept with finite probability if } \frac{\rho(\mathbf{R}_m)}{\rho(\mathbf{R}_n)} < 1 \end{cases} \tag{3.5.14}$$

Because this definition involves the ratios of probabilities there is no need to worry about normalization of the distribution $\rho(\mathbf{R}_n)$. Combining the trial and acceptance probabilities, we find that,

$$\frac{P(\mathbf{R}_n, \mathbf{R}_m)}{P(\mathbf{R}_m, \mathbf{R}_n)} = \frac{P_{trial}(\mathbf{R}_n, \mathbf{R}_m) P_{accept}(\mathbf{R}_n, \mathbf{R}_m)}{P_{trial}(\mathbf{R}_m, \mathbf{R}_n) P_{accept}(\mathbf{R}_m, \mathbf{R}_n)} = \frac{\rho(\mathbf{R}_m)}{\rho(\mathbf{R}_n)} \tag{3.5.15}$$

and hence the detailed balance condition is satisfied as required.

Several points need to be emphasized regarding this algorithm. First, the walk must be allowed to come to equilibrium before the desired averages may be computed. Methods for judging equilibrium will vary with application, but typically one monitor the running average of a function, observing convergence to a steady state value (within statistical fluctuations). A second point is that if the move $\mathbf{Y}$ is rejected, one must again include the point $\mathbf{X}^{(k)}$ in the distribution, and *not* attempt a second move. A final point is that the distribution is normalized

to the total number of sample points M during the walk, not to unity. This normalization leads to division by M when obtaining averages of histograms.

Although the Metropolis algorithm was developed to describe the stochastic behavior of neutrons in fission-able material, it was Metropolis himself who first applied it to the quantum many-body problem, prompted by the arrival of increased computing power at Los Alamos in 1952. This work provided the base from which the modern variational and diffusion Monte Carlo methods have developed.

3.5.2 Importance Sampling

Monte Carlo calculations can be carried out using sets of random points picked from any arbitrary probability distribution. The choice of distribution obviously makes a difference to the efficiency of the method. In most cases, Monte Carlo calculations carried out using uniform probability distributions give very poor estimates of high dimension integrals and are not a useful method of approximation. In 1953, however, Metropolis et. al. (1953) introduced a new algorithm for sampling points from a given probability function. This algorithm enables the incorporation of "importance sampling" into Monte Carlo integration. Instead of choosing points from a uniform distribution, they are now choosen from a distribution which concentrates the points where the function being integrated is large. Eq.(3.5.1) can then be rewritten as

$$I = \int_a^b \frac{f(x)}{g(x)} g(x) dx, \tag{3.5.16}$$

where the function $g(x)$ is chosen to be a reasonable approximation to $f(x)$. The integral can be calculated by choosing the random points from the probability distribution $g(x)$ and evaluating $f(x_i)/g(x_i)$ at these points. To enable $g(x)$ to be act as a distribution function it must be of one sign everywhere, and the

best possible choice[1] is $g(x) = |f(x)|$. The average of these evaluations gives an estimate of I. Another way of looking at this new integral is to define $dy = g(x)dx$, in which case

$$I = \int_A^B \frac{f(x(y))}{g(x(y))} dy \tag{3.5.17}$$

where the limits of integration are changed to correspond to the change of variable. In this case, random points are chosen from a uniform distribution in the domain $A < y < B$. The new integrand, f/g, is close to unity and so the variance for this function is much smaller than that obtained when evaluating the function by sampling from a uniform distribution. Sampling from a non-uniform distribution for this function should therefore be more efficient than doing a crude Monte Carlo calculation without importance sampling.

3.5.3 Correlated Sampling

Wave-function optimization is one of the most critical, time consuming and important stages of a VMC calculation. In VMC calculations, the accuracy of the trial wave-function limits the statistical efficiency of the calculation and the final accuracy of the result obtained. Therefore, several variational parameters are put into the trial wave-function. As more and more parameters are put into the wave-function the accuracy needed to obtain statistically significant improvements becomes more demanding and time-consuming. We wish of course to limit the number of parameters by choosing the trial functions as wisely as possible, but as the systems grow larger the number of parameters needed is increasing.

The straightforward approach to optimize the parameters numerically, is to use well established statistical tools to fit a surface to a set of data-points chosen by the user. The minimum of the surface can then be obtained. This

[1]The choice of $g(x) = |f(x)|$ minimizes the variance of the estimate of the integral.

procedure, however, is not very efficient. First, the data points are statistical and we therefore need several (or a few very accurate) data points to be able to significantly pinpoint a parameter minimum. Further, we must choose the shape of the surface. Close to the minimum, a parabolic surface would be a good approximation, but as we do not know where the minimum is we must use intuition and insight to choose the shape of the surface. We want a procedure that is fast and able to localize the minimum without much effort. Therefore, we have incorporated an optimizing procedure commonly used in the literature known as *correlated sampling*. Introduction of *guiding functions*, $\Psi_{\alpha'}$, allows the same random walk to produce several *local* estimates of the integral,

$$\langle E \rangle_{\alpha'} = \frac{\int |\Psi_{\alpha'}(\mathbf{X})|^2 E_L^{\alpha'}(\mathbf{X}) d\tau}{\int |\Psi_{\alpha'}(\mathbf{X})|^2 d\tau}. \tag{3.5.18}$$

Each of these local estimates of energy $\langle E \rangle_{\alpha'}$ must be in the neighborhood of the *central* parameter set α in parameter space. By the central parameter set we mean the set that produces the random walk by means of the Metropolis algorithm. Multiplication of

$$1 = \frac{|\Psi_\alpha(\mathbf{X})|^2}{|\Psi_\alpha(\mathbf{X})|^2} \tag{3.5.19}$$

inside the integrals of both the numerator and the denominator yields

$$\langle E \rangle_{\alpha'} = \frac{\int \omega_{\alpha,\alpha'}(\mathbf{X}) E_L^{\alpha'}(\mathbf{X}) |\Psi_\alpha(\mathbf{X})|^2 d\tau}{\int \omega_{\alpha,\alpha'}(\mathbf{X}) |\Psi_{\alpha'}(\mathbf{X})|^2 d\tau}, \tag{3.5.20}$$

with

$$\omega_{\alpha,\alpha'}(\mathbf{X}) = \frac{|\Psi_{\alpha'}(\mathbf{X})|^2}{|\Psi_\alpha(\mathbf{X})|^2} \tag{3.5.21}$$

By dividing with the norm,

$$N_\alpha = \int |\Psi_\alpha(\mathbf{X})|^2 \tag{3.5.22}$$

in both the numerator and the denominator we have

$$\langle E\rangle_{\alpha'} = \frac{\int \omega_{\alpha,\alpha'}(\mathbf{X}) E_L^{\alpha'}(\mathbf{X})\rho_\alpha(\mathbf{X})d\tau}{\int \omega_{\alpha,\alpha'}(\mathbf{X})\rho_\alpha(\mathbf{X})d\tau}, \tag{3.5.23}$$

with

$$\rho_\alpha(\mathbf{X}) = \frac{|\Psi_\alpha(\mathbf{X})|^2}{\int |\Psi_\alpha(\mathbf{X})|^2 d\tau} \tag{3.5.24}$$

Here $\rho_\alpha(\mathbf{X})$ is the probability distribution of the central parameter set. The random walk of the cental parameter set may therefore be used to generate estimates of several local variations in parameter space. We arrive at

$$\langle E\rangle_{\alpha'} \approx \frac{\sum_{i=1}^{M} \omega_{\alpha,\alpha'}(\mathbf{X}_i) E_L^{\alpha'}(\mathbf{X}_i)}{\sum_{i=1}^{M} \omega_{\alpha,\alpha'}(\mathbf{X}_i)} \tag{3.5.25}$$

where the sample points are taken from the distribution $\rho_\alpha(\mathbf{X})$ given by Equation (3.5.24).

This approach, in theory, looks very promising, but in fact it poses a few problems. The weights $\omega_{\alpha,\alpha'}$ may vary by several orders of magnitude, especially close to the nodes. The sample points generated by the Metropolis algorithm depends only on the cental wave-function. If the value of the central wave-function is small compared to the local wave-function, it implies that the value of the weight becomes large. This manifests itself near the nodes due to lack of more complicated many-body correlations. This could lead to a few sample points dominating the estimate of the integral. These few dominant points, may give really poor estimates of for example the energy, as the trial wave-functions fail to cancel divergent terms. Also, if the nodes of the local variation do not coincide with the nodes of the central wave-function we may actually allow sampling at the nodes.

Nevertheless, the introduction of guiding functions allows a fast and effective routine for optimizing the wave-function. A thorough investigation of the numerical instabilities induced by the introduction of guiding functions is given by Kent (Kent, Ph.D. Thesis, 1999).

3.6 Evaluation of Statistical Error in MC Simulations

The importance of probability density function is the fact that one can define the expectation value of a random variable (x) or a function ($g(x)$) which argument is random number as:

$$E_p(x) \equiv \overline{x} = \int_{-\infty}^{\infty} p(x')x'dx' \tag{3.6.1}$$

$$E_p[g(x)] \equiv \overline{g} = \int_{-\infty}^{\infty} p(x')g(x')dx' \tag{3.6.2}$$

$\overline{x}$ and $\overline{g}$ expressions are real mean values that we are interested in and investigate good approximate results by MC simulation.

The average the powers of the deviations of any random variable's possible values from its expected value (mean) is defined as "*central moment*":

$$n^{th}\text{central moment} = \overline{(x-\overline{x})^n} \tag{3.6.3}$$

The first central moment is zero. The second central moment is an important one which is known as *variance*:

$$var(x) = \sigma^2(x) = \overline{(x-\overline{x})^2} = \int p(x')(x'-\overline{x})^2 dx' \tag{3.6.4}$$

The positive square root of the variance gives the standart deviation:

$$\sigma(x) = [var(x)]^{1/2} \tag{3.6.5}$$

The expectation value of any $f(x)$ function between x_1 and x_2 in terms of $p(x)$ probability density function is found as:

$$I = E_p[f(x)] = \int_{x_1}^{x_2} dx p(x) f(x) \tag{3.6.6}$$

In the general case the probability density function is determined in the finite range of [a,b]:

$$\int_a^b p(x) = 1, \qquad p(x) > 0, \quad a < x < b \tag{3.6.7}$$

Then Equation 3.6.6 can be rewritten as:

$$\begin{aligned} \int_{x_1}^{x_2} dx p(x) f(x) &= \int_a^b dx p(x) f'(x) \\ &= \int_a^{x_1} dx p(x) f'(x) + \int_{x_1}^{x_2} dx p(x) f'(x) + \int_{x_2}^b dx p(x) f'(x) \end{aligned} \tag{3.6.8}$$

where $f'(x)$ function is defined as:

$$f'(x) = \begin{cases} 0, & a \le x \le x_1 \\ f(x), & x_1 \le x \le x_2 \\ 0, & x_2 \le b \end{cases} \tag{3.6.9}$$

or

$$f'(x) = \theta(x - x_1)\theta(x_2 - x) f(x).$$

Then the expression 3.6.8 can be re-arranged as:

$$I = \int_a^b dx p(x) \theta(x - x_1)\theta(x_2 - x) f(x) \tag{3.6.10}$$

Here, if $g(x) = \theta(x - x_1)\theta(x_2 - x)f(x)$ then:

$$I = \int_a^b dx p(x) g(x) \tag{3.6.11}$$

According to definition 3.6.6, Equation 3.6.11 gives the expectation value of the function $g(x)$. Let us define a $p_*(x)$ probability density distribution function which is different from $p(x)$:

$$\int_a^b p_*(x) dx = 1 \tag{3.6.12}$$

$$I = E_p[g(x)] = \int_a^b dx p(x) g(x) = \int_a^b dx p_*(x) \left[\frac{p(x)}{p_*(x)}\right] g(x) \tag{3.6.13}$$

$$I = \int_a^b dx p_*(x) \omega(x) g(x), \qquad \omega(x) = \frac{p(x)}{p_*(x)} \tag{3.6.14}$$

$$I = E_{p_*}[g(x)\omega(x)] = \int_a^b dx p_*(x) g(x) \omega(x) \tag{3.6.15}$$

As consequence:

$$I = E_p[g(x)] = E_{p_*}[g(x)\omega(x)] \tag{3.6.16}$$

Equation 3.6.16 is the exact determinist result.

Let's write Equation 3.6.6 n_p times and sum these expressions:

$$\begin{aligned} n_p I &= \sum_1^{n_p} \int_a^b dx_i p(x_i) g(x_i) \\ &= \int_a^b dx_1 p(x_1) g(x_1) + \int_a^b dx_2 p(x_2) g(x_2) + ... + \int_a^b dx_{n_p} p(x_{n_p}) g(x_{n_p}) \end{aligned} \tag{3.6.17}$$

Since $p(x)$ is probability density function:

$$\prod_{i=1}^{n_p} \left[\int_a^b dx_i p(x_i)\right] = 1 \tag{3.6.18}$$

$$n_p I = \prod_{i=1}^{n_p} \left[\int_a^b dx_i p(x_i) \right] \left[\sum_{i=1}^{n_p} g(x_i) \right] \tag{3.6.19}$$

$$I = \int_a^b dx_1 p(x_1) \int_a^b dx_2 p(x_2) ... \int_a^b dx_{n_p} p(x_{n_p}) \left\{ \frac{1}{n_p} \sum_{i=1}^{n_p} g(x_i) \right\} \tag{3.6.20}$$

As a result;

$$E_p[g(x)] = \int_a^b dx p(x) g(x) \tag{3.6.21}$$

$$E_{n_p,p}[g(x)] = \frac{1}{n_p} \sum_{i=1}^{n_p} g(x_i) \tag{3.6.22}$$

Expression 3.6.21 is an exact determinist expression for I, while 3.6.22 is an approximate result obtained over random positions generated according to $p(x)$ distribution.

$$E_p[E_{n_p,p}[g(x)]] = \int_a^b dx_1 p(x_1) \int_a^b dx_2 p(x_2) ... \int_a^b dx_{n_p} p(x_{n_p}) E_{n_p,p}[g(x)] \tag{3.6.23}$$

$$Var(E_{n_p,p}[g(x)]) = E_p \left[(E_{n_p,p}[g(x)] - E_p[E_{n_p,p}[g(x)]])^2 \right] \tag{3.6.24}$$

$$Var \left[\frac{1}{n_p} \sum_{i=1}^{n_p} g(x_i) \right] = \sum_{i=1}^{n_p} Var \left(\frac{g(x_i)}{n_p} \right) = \frac{1}{n_p} Var(g(x)) \tag{3.6.25}$$

$$Var[E_{n_p,p}(g(x))] = \frac{1}{n_p} Var[g(x)] \tag{3.6.26}$$

Similarly, the variance of expectation value over n_{p*} positions generated randomly from $p_*(x)$ distribution is written as:

$$E_{n_{p*},p_*}[g(x)\omega(x)] = I_{n_{p*},p_*} \approx I \tag{3.6.27}$$

$$Var_{p_*}[I_{n_{p*},p_*}] = \frac{1}{n_{p_*}} Var_{p_*}[g(x)\omega(x)] \tag{3.6.28}$$

Finally, standart deviation of the expected value $I = I \pm \sigma_I$ is found as:

$$\sigma_I = \frac{1}{\sqrt{n_p}} \sigma_{p,g}, \qquad \sigma_I = \frac{1}{\sqrt{n_{p_*}}} \sigma_{p_*,gw} \tag{3.6.29}$$

CHAPTER FOUR
QUANTUM MONTE CARLO METHODS

4.1 Variational Quantum Monte Carlo

The variational quantum Monte Carlo (VMC) method is the simpler of the two quantum Monte Carlo methods used in this thesis. It is based on combination of the ideas described in the previous sections, namely the variational principle and Monte Carlo evaluation of integrals using importance sampling based on the Metropolis algorithm.

4.1.1 The Variational Principle

The Variational Principle provides the starting point for almost all methods which aim to find an approximate solution to Schrödinger's equation. It may be stated as follows:

> *The expectation value of a Hamiltonian, $\hat{H}$, calculated using a trial wave function, Ψ_T, is never lower in value than the true ground state energy, ε_0, which is the expectation value of $\hat{H}$ calculated using the true ground state wavefunction, Ψ_0.*

Obviously this is extremely valuable because it means that it is always possible to find an upper bound for the ground state energy. It is also possible to use variational methods to study excited states, but the real strength of this principle lies in finding ground state energies. Variational calculations rely on making a physically plausible guess at the form of the ground state wavefunction, Ψ_T, of the Hamiltonian, $\hat{H}$. This guess will be referred to as the

trial wavefunction throughout this thesis. The "trial" part of the name refers to the use of the wavefunction as a guess of the true groundstate wavefunction to be used as the input wavefunction in a Variational quantum Monte Carlo (VMC) calculation. The trial wavefunction depends on a number of variable parameters which can be adjusted to minimise the energy expectation value. If the guessed values of these parameters are good and the chosen functional form builds in enough variational freedom to adequately describe the physics of the system being studied, the very accurate estimates of the ground state energy can be obtained. Variational Monte Carlo (VMC) calculations are direct applications of the above variational principle.

The expectation value of the exact groundstate wavefunction, Ψ_0, with this Hamiltonian, is the exact groundstate energy.

$$\begin{aligned} E_0 &= \frac{\langle \Psi_0 | \hat{H} | \Psi_0 \rangle}{\langle \Psi_0 | \Psi_0 \rangle} \\ &= \int \frac{\Psi_0^*(\mathbf{R}) \hat{H} \Psi_0(\mathbf{R}) d\mathbf{R}}{\Psi_0^*(\mathbf{R}) \Psi_0(\mathbf{R}) d\mathbf{R}} \end{aligned} \tag{4.1.1}$$

where $\mathbf{R}$ denotes the 3N-dimensional vector of electronic positions. The VMC method relies on one being able to construct a trial wavefunction, Ψ_T, that is a reasonably good approximation to the true groundstate wavefunction, Ψ_0. More information about selection of trial wavefunctions is given in chapter 5. The energy associated with the trial wavefunction is given by,

$$\begin{aligned} E_T &= \frac{\langle \Psi_T | \hat{H} | \Psi_T \rangle}{\langle \Psi_T | \Psi_T \rangle} \\ &= \int \frac{\Psi_T^*(\mathbf{R}) \hat{H} \Psi_T(\mathbf{R}) d\mathbf{R}}{\Psi_T^*(\mathbf{R}) \Psi_T(\mathbf{R}) d\mathbf{R}} \end{aligned} \tag{4.1.2}$$

The variational principle, described above, ensures that the energy, E_T, is a rigorous upper bound to the true ground-state energy, E_0.

The VMC method is a Monte Carlo method for evaluating the multi-dimensional integral in Eq.4.1.2. This is achieved by rewriting Eq.4.1.2 in the following form,

$$E_T = \int \frac{|\Psi_T(\mathbf{R})|^2 \frac{\hat{H}\Psi_T(\mathbf{R})}{\Psi_T(\mathbf{R})} d\mathbf{R}}{\int \Psi_T(\mathbf{R}) d\mathbf{R}} \tag{4.1.3}$$

The Metropolis algorithm is used to sample a series of points, $\mathbf{R}$, in configuration space. At each of these points the "Local Energy", $E_L = \frac{\hat{H}\Psi_T(\mathbf{R})}{\Psi_T(\mathbf{R})}$, is evaluated. After a sufficient number of evaluations of the local energy have been made, the average is taken in the same way as in Eq.3.5.2.

$$E_{\mathrm{VMC}} = \frac{1}{N} \sum_{i=1}^{N} \frac{\hat{H}\Psi_T(\mathbf{R}_i)}{\Psi_T(\mathbf{R}_i)} \tag{4.1.4}$$

where the Metropolis algorithm ensures that in the limit of large N, the $\mathbf{R}_i$ are sampled from $|\Psi_T(\mathbf{R})|^2$.

Figure 5.1 is a schematic flow chart illustrating how a typical VMC algorithm works. There are two distinct parts to the algorithm; an initial equilibration stage and an energy evaluation stage. During the initial equilibration stage, the walker is moved according to the Metropolis algorithm, but the local energy is not accumulated along the walk. This stage is required because the initial starting point of the walker is chosen randomly and therefore a set of Metropolis moves are required before the average along its walk is correctly sampling the distribution, $|\Psi_T|^2$. The required number of equilibration steps can be established by calculating the energy at each step from the beginning of the random walk and looking for the point at which there is no longer a drift in the average value of the local energy. During the energy evaluation stage, the energy of the walker is accumulated after each move.

The advantage of Metropolis algorithm is that it only requires evaluating Ψ for the proposed move; the unknown normalization $\int \Psi^2 dx$ is not required. Initially,

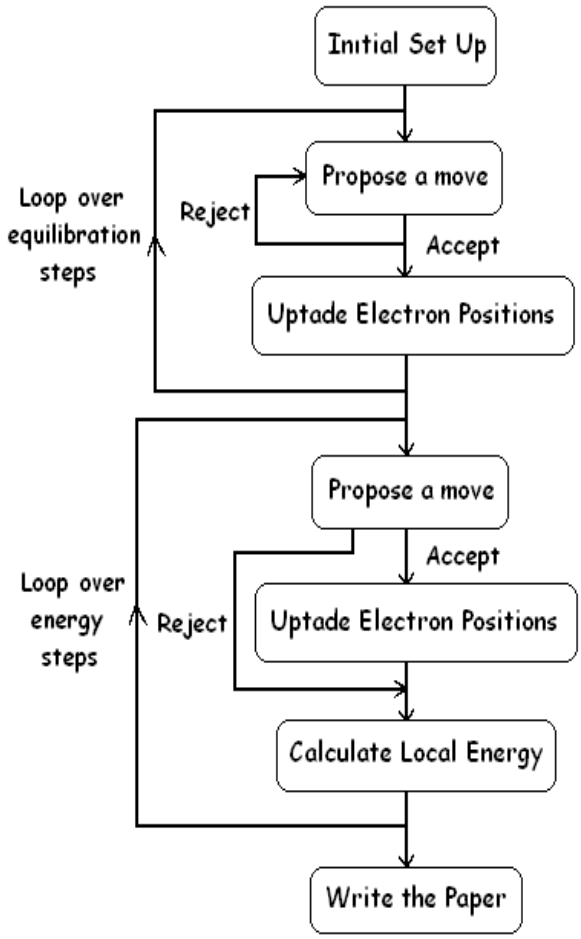

Figure 4.1 Flow chart illustrating the VMC algorithm.

one must wait for equilibrium (i.e. for convergence to the distribution Ψ^2) before computing any expectation values. Equilibration can be judged by looking for a systematic trend in $\langle E_L \rangle$ over the course of the walk. Other quantities of interest also can be sampled at the same time. In choosing the step size, one wishes to maximize the actual *accepted* step size. Attempting too large a step will result in a small acceptance to rejection ratio, and so actual movement will be small. Note attempting large enough moves clearly also will restrict the actual movement. This step size should therefore be optimized empirically based on the observed

behavior of the sampling algorithm.

In the above algorithm we have moved and accepted or rejected one electron at a time. One also could have moved all the electrons at once, and then accepted or rejected the move as a whole. Moving one electron at a time is often more efficient, especially with the wave function forms typically used in which the one-electron contribution to Ψ and E_L can be evaluated efficiently.

4.2 Monte Carlo Diagonalization Method

The basic principle in the MCD method is the same as in the exact diagonalization (ED) method. The only difference between ED and MCD is in the evaluation of matrix elements. In the ED method, the evaluation is done analytically, requiring simple functional form for the basis functions. In the MCD method, the matrices are evaluated statistically, and there are no restrictions on the basis functions at all. On the other hand, the number of basis functions required to achieve convergence for the Schrödinger equation is often orders of magnitude larger in the ED method than in the MCD method (Siljamäki, 2005). It should pointed out that the enhancement of particles in ED method lead to an exponential increase in the size of basis set, then the number of efficiently treated particles is quite restrictive. In principle the approach seems ideal for solving interacting few-body systems, but in practice only very small number of particles can be calculated with good accuracy ($N \lesssim 10$) (Maksym, 2005). On the other hand, the matrix elements for corresponding system are calculated analytically. Thus, in the case of any changes in Hamiltonian or basis functions matrix elements have to be regenerated. Usually it is not easy to obtain analytical result for integrals of matrix elements. Compared to ED method, it should be simple enough to make any changes in the corresponding system and to implement calculations for larger number of particles feasible in the MCD method. Moreover,

this numerical method can be applied to yield the eigenfunctions and eigenvalues for both the ground and excited states of the exciton.

The technique is simple and straightforward to apply. Any trial wavefunction for the solution of Schrödinger equation of the corresponding system can be written as expansion of basis functions (ψ_p):

$$\Psi_T = \sum_{p=0}^{N_p} C_p \psi_p \tag{4.2.1}$$

Symbolically the Schrödinger equation is:

$$\mathcal{H}\Psi_T = \varepsilon \Psi_T \tag{4.2.2}$$

$$\sum_{p=0}^{N_p} C_p H \psi_p = \varepsilon \sum_{p=0}^{N_p} C_p \psi_p \tag{4.2.3}$$

Multiplying the equation 4.2.3 by $\Psi_T^* = \sum_{p'} C_{p'}^* \psi_p^*$ on the left and then integrating over the space we get:

$$\sum_p \sum_{p'} C_{p'}^* C_p \int \psi_{p'}^* H \psi_p d\tau = \varepsilon \sum_p \sum_{p'} C_{p'}^* C_p \int \psi_{p'}^* \psi_p d\tau \tag{4.2.4}$$

According to minimization principle:

$$\frac{\partial \varepsilon}{\partial C_k^*} = \sum_{p',p} \delta_{p',k} C_p (\langle \psi_{p'} | H | \psi_p \rangle - \varepsilon \langle \psi_{p'} | \psi_p \rangle) = 0 \tag{4.2.5}$$

$$\sum_{p=0}^{N_p} C_p (\langle \psi_k | H | \psi_p \rangle - \varepsilon \langle \psi_k | \psi_p \rangle) = 0 \tag{4.2.6}$$

As a result the Schrödinger equation of the system can be written in matrix form as:

$$\overline{\overline{K}}\overline{C} = \varepsilon \overline{\overline{M}}\overline{C} \tag{4.2.7}$$

where $\overline{\overline{K}}$ and $\overline{\overline{M}}$ matrices are often called as stiffness and mass matrices, respectively. $\overline{C}$ is column matrix consisting from expansion coefficients (C_p). This generalized eigenvalue equation (4.2.7) is usually solved numerically.

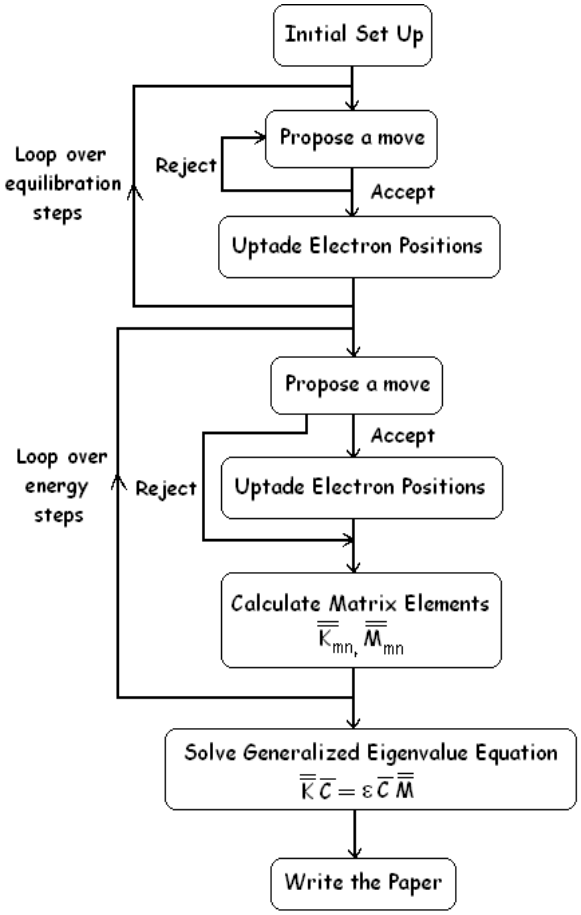

Figure 4.2 Flow chart illustrating the MCD algorithm.

4.2.1 Error Estimation in Monte Carlo Diagonalization Method

Stiffness and mass matrix elements (K_{ij}, M_{ij}) have been calculated according to correlated sampling technique described in section 3.6.3. The evaluation of

matrix elements are given in detail in section 6.2.3. Standart deviation corresponding to each multidimensional integral have been also estimated during Monte Carlo random walk by using Equation 3.6.29. Accordingly, the generalized eigenvalue equation (4.2.7) is implicitly in the following form:

$$(\overline{\overline{K}}_0 \pm \overline{\overline{\sigma}}_K)\overline{C}_0 = (\varepsilon_0 \pm \Delta\varepsilon)(\overline{\overline{M}}_0 \pm \overline{\overline{\sigma}}_M)\overline{C}_0 \tag{4.2.8}$$

where $\overline{\overline{K}}_0$ and $\overline{\overline{M}}_0$ are matrices obtained from correlated sampling MC results. The standart deviations calculated for corresponding multidimensional integrals form $\overline{\overline{\sigma}}_K$ and $\overline{\overline{\sigma}}_M$ MC error matrices. The energy solution of generalized eigenvalue problem is ε_0 ant it has $\Delta\varepsilon$ standart deviation due to random number process. Although we do not evaluate the expansion coefficients, C_p, these also have uncertainty σ_C, which we have neglected. Since the matrices of size 8 are treated in calculations in this thesis and statistical errors in $\overline{\overline{\sigma}}_K$ and especially in $\overline{\overline{\sigma}}_M$ matrices are reasonably small. Hence, neglecting σ_C is a good approximation and enable to guess the MC statistical error to a good extent. Good agreement between our results and previous studies explain in chapter 6 justifies our prediction.

After some arrangements in Equation (4.2.8) we find the following expression:

$$\overline{\overline{K}}_0\overline{C}_0 \pm \overline{\overline{\sigma}}_K\overline{C}_0 = \varepsilon_0\overline{\overline{M}}_0\overline{C}_0 \pm \varepsilon_0\overline{\overline{\sigma}}_M\overline{C}_0 \pm \Delta\varepsilon\overline{\overline{M}}_0\overline{C}_0 \pm \Delta\varepsilon\overline{\overline{\sigma}}_M\overline{C}_0 \tag{4.2.9}$$

$$\pm(\overline{\overline{\sigma}}_K - \varepsilon_0\overline{\overline{\sigma}}_M)\overline{C}_0 = \pm\Delta\varepsilon(\overline{\overline{M}}_0 \pm \overline{\overline{\sigma}}_M)\overline{C}_0 \tag{4.2.10}$$

Then, possible $\pm\sigma_i$ $(i = K, M)$ configurations lead to four energy solutions. The differences between maximum and minimum values and ε_0 give $\Delta\varepsilon_{\max}$ and $\Delta\varepsilon_{\min}$ errors in evaluation of ε_0 by Monte Carlo Diagonalization method.

$$\varepsilon_0 - \Delta\varepsilon_{\min} < \varepsilon_{\mathrm{MCD}} < \varepsilon_0 + \Delta\varepsilon_{\max} \tag{4.2.11}$$

CHAPTER FIVE
VARIATIONAL TRIAL WAVE FUNCTIONS

Important to both VMC and MCD is the choice of the trial function. In VMC, all averages are evaluated with respect to the trial function, and so it determines the ultimate accuracy.

Most variational methods rely on a double basis-set expansion in 1-electron primitive functions and in N-electron Slater determinants (Hammond, Lester, & Reynolds, 1994). A unique characteristic of Monte Carlo methods is their ability to use arbitrary wave function forms - including ones with explicit interelectronic distance dependencies - enabling treatments beyond forms constructed solely with one-electron functions (Ferguson, Siepmann, & Truhlar, 1998). Given this flexibility, it is important to recall properties a trial function ideally should possess. Thus, in this section we first review the known properties of exact solutions of the Schrödinger equation. The various forms of approximate, currently used trial functions are discussed.

5.1 Properties of Exact Wave Function

What do we know about the exact wave function, Φ_0? By definition, it satisfied $\mathcal{H}\Phi_0 = E_0\Phi_0$. For bound electronic states, we know that in the absence of external fields Φ_0 can be made real and is square integrable. An important corollary of the eigenvalue equation is that the local energy is a constant for an eigenstate. For non-eigenstates, the variance of the local energy is an important measure of wave function quality. It is used to help optimize the trial wave function. All the above are global properties of Φ_0 (Hammond, Lester, & Reynolds, 1994).

We also know several local properties of Φ_0, in addition to the above global

properties. For example, because the local energy is a constant everywhere in space, each singularity of the Coulomb potential must be cancelled by a corresponding term in the local kinetic energy. This condition results in a *cusp*, i.e., a discontinuity in the first derivative of Φ_0 where two charged particles meet. With a sufficiently flexible trial wave function one can include appropriate degrees of freedom which are then determined by the *cusp condition*.

5.2 General Trial Function Forms

The exact wave function can be approximated in a number of ways through series expansions in the electronic coordinates. The convergence of these series depends upon the type of terms included. Hylleraas and Pekeris has great success for He with trial functions of the form

$$\Psi_{\text{Hylleraas}} = (\sum_{k=1}^{N} d_k r^{a_k} s^{b_k} t^{e_k}) e^{-\frac{1}{2}}, \tag{5.2.1}$$

where r is the electron-electron separation (which we have previously designated as r_{ij}), $s = r_1 + r_2$, and $t = r_1 - r_2$. Here r_1 and r_2 are the scalar distances of the electrons from the nucleus. The electron-nucleus cusp condition is satisfied by the exponential term, and the electron-electron cusp is satisfied by choosing the proper values for the coefficients. Because all the interparticle distances are represented, very accurate descriptions of the He wave function may be obtained with relatively few terms. Although Equation 5.2.1 is written explicitly for two electrons, it is readily generalized to larger systems (Ruiz, 2004). More complicated forms of Ψ have been examined, motivated primarily by the goal of satisfying the various n-body coalescences. These forms are summarized in Table 5.1.

Helium has long served as a testing ground for atomic trial functions because

Table 5.1 Selected forms of many-electron wave functions with explicit interelectron distance dependence. (Hammond, Lester, & Reynolds, 1994 and references therein.)

Form	Ψ
Hylleraas	$e^{-\epsilon s}\sum_{\mu} c_\mu r^{l_\mu} s^{m_\mu} t^{n_\mu}$
Conroy	$\sum_{\mu} \frac{r_{12}^{\mu}}{n!(n+1)!} e^{b\sum_{i<j}(r_1^2+r_2^2+r_{12}^2)(r_1^2+r_2^2+2s)^{-1/2}} \sum_{mn} C_{mn}\varphi_m(1)\varphi_n(2)$
Ho	$e^{\epsilon(r_1+r_2+r_3)}\sum_{\mu} c_\mu r_1^{l_\mu} r_2^{m_\mu} r_3^{n_\mu} r_{12}^{p_\mu} r_{13}^{q_\mu} r_{23}^{s_\mu}$
Frankowski & Pekeris	$e^{\epsilon s}\sum_{\mu} c_\mu r^{l_\mu} s^{m_\mu} t^{n_\mu} [(r_1^2+r_2^2)\ln(r_1^2+r_2^2)]$
Baker & Morgan	$e^{\epsilon s}\sum_{\mu} c_\mu r^{l_\mu} s^{m_\mu} t^{n_\mu} (\ln s)^{i_\mu} \sinh^{j_\mu}(b_\mu t)\cosh^{k_\mu}(b_\mu t)$

of its simplicity. One measure the quality of a trial function form is the rate of convergence of the variational energy with the number of terms in the series. For example, a nine-term Hylleraas function yields an energy of -2.9035 hartrees, while a 1078 term function yields -2.903724375 hartrees. Clearly, convergence is not fast. On the other hand, by adding terms with powers of $\ln s$ and negative powers of s, one can obtain -2.903724377033 hartrees with only 246 terms. The functional form clearly is very important. It was argued that comparable accuracy in a CI calculation would require 2×10^5 one-electron basis functions and approximately 7×10^{12} configurations (Hammond, Lester, & Reynolds, 1994).

Even though such accuracy is not typically sought, electron-correlation terms may provide clues for constructing Ψ's for many-electron systems. The difficulty with these general expansions for larger atoms and molecules is in constructing

the correct spatial and exchange symmetries. Moreover, even with Monte Carlo integration, the task of determining hundreds or thousands of parameters remains an obstacle.

5.2.1 Hartree Fock and Beyond

Unlike the forms just discussed, the most widely used methods in *ab initio* electronic structure theory are based on molecular orbital (MO) expansions and the Hartree-Fock approximation. MO theory has been the foundation for most chemical concepts during the past 50 years. As a first approximation, the N-electron wave function $\Phi(\mathbf{x}_1, ..., \mathbf{x}_N)$ is represented by a Slater determinant of spin orbitals. It often is abbreviated by writing only the diagonal elements of the Slater matrix, namely,

$$\Psi_D = \det \begin{vmatrix} \tilde{\varphi}_1(\mathbf{x}_1) & \cdots & \tilde{\varphi}_1(\mathbf{x}_n) \\ \vdots & \ddots & \vdots \\ \tilde{\varphi}_n(\mathbf{x}_1) & \cdots & \tilde{\varphi}_n(\mathbf{x}_n) \end{vmatrix} \equiv \det |\tilde{\varphi}_1(\mathbf{x}_1) \cdots \tilde{\varphi}_n(\mathbf{x}_n)| \tag{5.2.2}$$

Each spin orbital, $\tilde{\varphi}_i$, consists of a spatial function, φ_i, multiplied by an electron spin function (α or β). The orbital approach is motivated by a simple generalization of the one-electron description of the H atom, building in the antisymmetry required by the Pauli principle. The determinantal part of the probability distribution, Ψ_D^2, depends on the product $\varphi_1^2\varphi_2^2 \cdots \varphi_n^2$ of one-electron probabilities. Since no terms involve conditional probabilities of two or more electrons, each particle acts independently of the others in this type of wave function, and the total probability is a simple product of one article probabilities. This *independent-particle* approximation differs fundamentally from Hylleraas-type functions which include r_{ij} terms explicitly.

5.2.2 Correlated Molecular Orbital Functions

In the above discussion we have learned the importance of r_{ij} terms. On the other hand Hartree-Fock and post Hartree-Fock wave functions, which do not explicitly contain these terms, lead to molecular integrals that are substantially more convenient for integration. At present, the vast majority of work is done with the latter independent-particle-type functions. Correlated molecular orbital (CMO) methods incorporate the best of both (Hammond, Lester, & Reynolds, 2004).

Although there are many ways one might construct such CMO functions, typically they are constructed as a determinant of orbitals where each orbital is multiplied by a function of the interelectronic coordinates $f(r_{ij}) \equiv f_{ij}$. Explicitly,

$$\Psi_{\mathrm{CMO}} = \mathcal{A}\varphi_1(\mathbf{x}_1)\varphi_2(\mathbf{x}_2)\cdots\varphi_n(\mathbf{x}_n)f_{12}f_{13}\cdots f_{n-1,n}, \tag{5.2.3}$$

where $\mathcal{A}$ is the antisymmetrizer operator. Most often the form of f_{ij} is independent of orbitals, making Ψ_{CMO} a simple product function

$$\Psi_{\mathrm{CMO}} = \Psi_D\Psi_C, \tag{5.2.4}$$

where Ψ_D is the determinantal part and Ψ_C is a product of correlated functions.

We can distinguish between two classes of functions Ψ_C. In the first class, Ψ_C contains polynomials in r_{ij}, similar to the Hylleraas functions. The second class is an exponential or Jastrow form

$$\Psi_C e^U \tag{5.2.5}$$

where U contains all the r_{ij} dependence. Representatve functional forms are shown in Table 5.2. Note that each form contains one or more parameters which

can be used to represent the two-electron cusp.

As an example, consider the most commonly used form in QMC, the Padé-Jastrow function,

$$U = \sum_{i=1}^{N} \sum_{j<i}^{N} \frac{a_1 r_{ij} + a_2 r_{ij}^2 + \cdots}{1 + b_1 r_{ij} + b_2 r_{ij}^2 + \cdots} \tag{5.2.6}$$

The general behavior of e^U is shown in Figure 5.1, beginning at unity for $r_{ij} = 0$

Table 5.2 Comparison of different forms of the Jastrow U function (Hammond, Lester, & Reynolds, 1994 and references therein).

Form	U
Padé-Jastrow	$\sum_{i,j,A} \frac{P(r_{iA},r_A,r_{ij})}{1+Q(r_{iA},r_A,r_{ij})}$
Boys-Handy	$\sum_{ij}\sum_{\mu} c_\mu \left(\frac{a_{1\mu} r_{iA}}{1+b_{1\mu} r_{iA}}\right)^{u_\mu} \left(\frac{a_{2\mu} r_{iA}}{1+b_{2\mu} r_{iA}}\right)^{\upsilon_\mu} \left(\frac{a_{3\mu} r_{ij}}{1+b_{3\mu} r_{ij}}\right)^{\omega_\mu}$
Double exponential	$-\sum_{ij} b e^{-a r_{ij}}$
Gaussian geminal	$\sum_{ij}\sum_{\mu} a_\mu r_{ij}^2$

and asymptotically approaching a constant value for large r_{ij}. In the simplest case, where only a_1 and b_1 are non-zero, this asymptotic value is $\exp(a_1/b_1)$. One can verify that the electron-electron cusp condition requires a_1 to be $1/2$ for unlike spins and $1/4$ for like spins.

The linear Padé-Jastrow form has only one free parameter, namely b_1, with which to optimize the wave function. Such Jastrow-type functions have the desirable property that they do not change the nodes created by the determinantal factor, because the correlation functions are positive everywhere.

However, their use does not have an undesired side effect. Using an SCF determinant and multiplying by Ψ_C causes a global expansion of the electron density. If we assume that the SCF density is relatively accurate, then one needs to rescale the trial function to re-adjust the density. This can be accomplished simply by multiplying by an electron-nucleus Jastrow function. If U for this Jastrow function is given by

$$U = -\sum_{i=1}^{N}\sum_{A=i}^{N_{nuc}} \frac{\lambda_1 r_{iA} + \lambda_2 r_{iA}^2 + \cdots}{1 + \nu_1 r_{iA} + \nu_2 r_{iA}^2 + \cdots}, \tag{5.2.7}$$

then, as for electron-electron function, λ_1 is determined by the cusp condition.

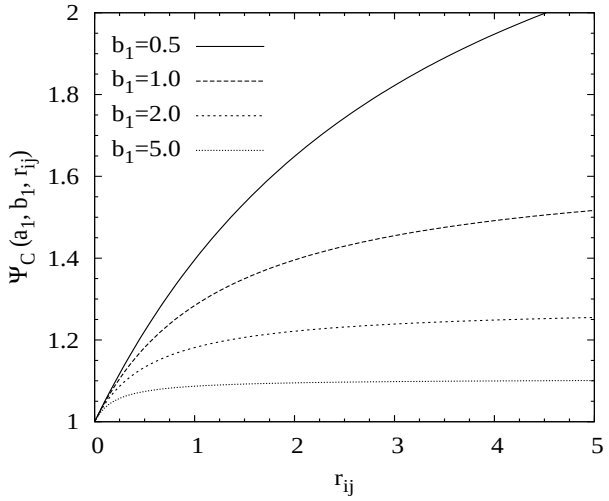

Figure 5.1 Dependence of linear Padé-Jastrow function on r_{ij}. The coefficient a_1 is set to 0.5 to satisfy the electron-electron cusp condition.

For CMO wave functions one can optimize the Jastrow parameters, the molecular orbital coefficients, and the atomic orbital exponents. Clearly, practical limitations will be reached for very large systems, but such optimization has been done for several systems. A 21 parameter function, that included all combinations of r_i, r_j, and r_{ij} to fourth order, including electron-electron-nucleus terms, obtained essentially all the correlation energy for two-electron systems, 99% of the correlation energy for Be, and 86% of the correlation energy for Ne.

These results are impressive, and show that VMC can be an attractive quantum chemistry technique in its own right.

5.3 Trial variational functions of this study

The trial variational wave functions proposed to study ground state properties of two interacting particle confined by parabolic potential in 2D as well as 3D QDs have the general form of:

$$\Psi_T = \Phi F \tag{5.3.1}$$

Here Φ is constructed from exact eigenfunctions of noninteracting single particle Hamiltonian, which are well known harmonic oscillator eigenvectors.

$$\Phi(\gamma, r_i, r_j) = \phi(r_i)\phi(r_j), \qquad \phi(r_i) = \exp(-\frac{\gamma}{2} W r_i^2) \tag{5.3.2}$$

where γ is variational parameter and W is the frequency of parabolic confinement potential. r_i is the position vector of i.th particle.

F part in equation 5.3.1 is correlation function, which should describe the correlations between the particles correctly. Four different types of correlation functions have been used in the calculations: two of these are in exponential form and the the others are constructed as serial expansion in terms of Hylleraas-like coordinates multiplied by corresponding exponential forms.

- Simple exponential form:

$$F_1(\lambda, r_{ij}) = \exp(-\lambda r_{ij}) \tag{5.3.3}$$

- Jastrow factor:

$$F_2(a,b,c,r_{ij}) = J(a,b,c,r_{ij}) = \exp\left(\frac{ar_{ij} - br_{ij}^2}{1+cr_{ij}}\right) \tag{5.3.4}$$

- Simple exponential $\times$ Serial expansion term:

$$F_3(\lambda, r_i, r_j, r_{ij}) = \exp(-\lambda r_{ij}) \sum_{[n]} C_{[n]} r_i^{n_i} r_j^{n_j} r_{ij}^{n_{ij}} \tag{5.3.5}$$

- Jasrow factor $\times$ Serial expansion term:

$$F_4(a,b,c,r_i,r_j,r_{ij}) = \exp\left(\frac{ar_{ij} - br_{ij}^2}{1+cr_{ij}}\right) \sum_{[n]} C_{[n]} r_i^{n_i} r_j^{n_j} r_{ij}^{n_{ij}} \tag{5.3.6}$$

Here λ, γ, a, b, and c are positive variational parameters to be optimized. n denotes the set of numbers (n_i, n_j, n_{ij}). Note that $C_{[n]}$ linear expansion coefficients have been optimized via the variational principle.

5.4 Energy and Variance Optimization

Optimization of trial wave functions is critical tool for VMC as well as MCD calculations. The most used two approaches for optimizing the trial wave-functions are presented here. When optimizing we seek the parameter configuration of the trial wave-function Ψ_T that best approximates the behavior of the true eigenfunction. For the true ground state Ψ_0, a natural choice is to optimize with respect to *energy minimization*. Optimization with respect to variance is another natural choice in that for every eigenfunction, not just the ground state, the variance of the local energy vanishes. This means that a *variance optimization* scheme could be applied in finding any eigenstate, because we know in advance that the value of the variance should be zero.

The energy optimization scheme is based on the variational principle (introduced in section 4.1.1),

$$\langle E_L \rangle = \frac{\int \Psi_T^{*p} \hat{H} \Psi_T^p d\tau}{\int |\Psi_T^p|^2 d\tau} \geq E_0. \tag{5.4.1}$$

Here the fact that the variational energy provides an upper bound to the ground state energy is exploited. The parameters $p = \{p_1, p_2, ...\}$ which correspond to a global energy minimum, are chosen as the best fit to the true ground state wavefunction.

In the literature there is not any consensus that any optimization scheme provides the most stable approach, and superiority. The straightforward estimate of the uncorrelated variance is

$$\sigma = \frac{1}{M-1} \sum_{i=1}^{M} (E_{L,i} - \langle E_L \rangle)^2 \tag{5.4.2}$$

where $\langle E_L \rangle$ is the average of the individual samples $E_{L,i}$. Many have chosen instead to optimize,

$$\sigma = \frac{1}{M-1} \sum_{i=1}^{M} (E_{L,i} - E_{\text{ref}})^2 \tag{5.4.3}$$

where E_{ref} is taken to be as close to the expected average of the local energy as possible (Reine, Ph.D. Thesis, 2004).

The trial wave functions in this thesis have been optimized according to energy minimization scheme.

CHAPTER SIX
IMPLEMENTATION AND NUMERICAL RESULTS

6.1 Single electron quantum dot system

Hamiltonian H of N identical particles in the first quantization form:

$$H = H_0 + H_I \tag{6.1.1}$$

where H_0 is the sum of ith single particle Hamiltonian H_{0i} and H_I describes the interaction between them. Single particle Hamiltonian is:

$$H_{0i} = \frac{1}{2m^*}\left[\vec{p_i} + \frac{e}{c}\vec{A}_i\right]^2 + V(\vec{r_i}) - g\mu_B\vec{B}(\vec{r_i})\vec{\sigma_i} \tag{6.1.2}$$

where m^*, e and g are the effective mass, charge and the g-factor of the particle, and r_i, p_i and σ_i are the position, momentum and spin of ith particle, respectively. c and μ_B are speed of light and Bohr magneton. We assume a magnetic field $B = \mathrm{rot}\vec{A}$ and choose vector potential $\vec{A}$ in an appropriate gauge. $V(r)$ is the static scaler potential. Interaction Hamiltonian is:

$$H_I = \sum_{i<j} U(\vec{r_i} - \vec{r_j}) \tag{6.1.3}$$

with two particle interaction potential which depends only on the relative distance. We look forward to find a way to calculate energy levels and their wave functions of N particle system. There are only two exact solutions known up to now. One of which is trivial case, $N = 1$, and the other is the case of $N = 2$ where the Hamiltonian can be decoupled into that for the center-of-mass coordinate and for the relative-motion coordinate, each of which is a single particle Hamiltonian. We will soon discuss the detail of the exact solution of singe electron QD Hamiltonian The static confining potential $V(r)$ in equation

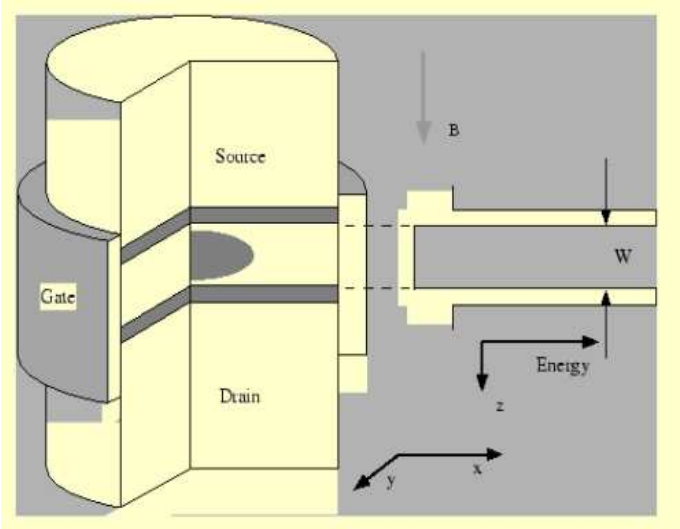

Figure 6.1 The schematics of vertically quantum dot (Taken from Ref. Tokura, 2000).

is made up of in-plane potential $V_{xy}(\rho)$ and vertical potential $V_z(z)$ ($\rho = (x, y)$). Moreover, we almost always consider the situation where the magnetic field is uniform and normal to $(x - y)$ plane, $\vec{B} = (0, 0, B)$. Therefore, the variables x, y and z are decoupled, $H_0 = H_{0\rho} + H_{0z}$ and the eigenfunction is the product of two;

$$\Psi_l(\vec{r}) = \phi_{n,m}(\rho)\xi_j(z) \tag{6.1.4}$$

and the eigenenergy is the sum $E_l = E_{n,m} + E_j$. The Zeeman energy term can be considered separately since we neglected the spin-orbit interaction.

We only consider that the in-plane potential $V_{xy}(\rho)$ has cylindrical symmetry. Then the symmetric gauge is convenient;

$$\vec{A} = \frac{B}{2}\rho\hat{e}_\varphi = \frac{B}{2}(-y, x, 0) \tag{6.1.5}$$

where $\rho = \sqrt{x^2 + y^2}$ and $\hat{e}_\varphi$ is unit vector to azimuthal direction. We took the coordinate origin to the cylindrical symmetry axis. First we consider the in-plane

component. The Hamiltonian is:

$$\begin{aligned} H_{0\rho} &= \frac{1}{2m^*}\left[\left(\frac{\hbar}{i}\vec{\nabla}\cdot+\frac{e}{c}\vec{A}\right)\left(\frac{\hbar}{i}\vec{\nabla}+\frac{e}{c}\vec{A}\right)\right]+V_{xy}(\rho) \\ &= \frac{1}{2m^*}\left[-\hbar^2\nabla^2-i\frac{\hbar e}{c}\vec{\nabla}\cdot\vec{A}-i\frac{\hbar e}{c}\vec{A}\vec{\nabla}+\frac{e^2}{c^2}A^2\right]+V_{xy}(\rho) \end{aligned}$$

According to cylindrical coordinates;

$$\begin{aligned} \vec{\nabla} &\longrightarrow \frac{\partial}{\partial\rho}\hat{e}_\rho+\frac{1}{\rho}\frac{\partial}{\partial\varphi}\hat{e}_\varphi \\ \vec{\nabla}\cdot &\longrightarrow \frac{1}{\rho}\frac{\partial}{\partial\rho}(\rho\hat{e}_\rho)+\frac{1}{\rho}\frac{\partial}{\partial\varphi}\hat{e}_\varphi \\ \nabla^2 &\longrightarrow \frac{1}{\rho}\frac{\partial}{\partial\rho}(\rho\frac{\partial}{\partial\rho})+\frac{1}{\rho^2}\frac{\partial^2}{\partial\varphi^2}+\frac{\partial^2}{\partial z^2} \end{aligned} \tag{6.1.6}$$

where $\hat{e}_\rho$ is unit vector to radial direction.

$$H_{0\rho}=-\frac{\hbar^2}{2m^*}\left\{\frac{1}{\rho}\frac{\partial}{\partial\rho}(\rho\frac{\partial}{\partial\rho})+\frac{1}{\rho^2}\frac{\partial^2}{\partial\varphi^2}\right\}-i\frac{\hbar e}{m^*c}\frac{B}{2}+\frac{1}{2m^*}\frac{e^2}{c^2}\frac{B^2\rho^2}{4}+V_{xy}(\rho) \tag{6.1.7}$$

We defined cyclotron frequency as $\omega_c=\frac{eB}{m^*c}$. Then;

$$H_{0\rho}=-\frac{\hbar^2}{2m^*}\left\{\frac{1}{\rho}\frac{\partial}{\partial\rho}(\rho\frac{\partial}{\partial\rho})+\frac{1}{\rho^2}\frac{\partial^2}{\partial\varphi^2}\right\}-i\frac{\hbar\omega_c}{2}\frac{\partial}{\partial\varphi}+\frac{1}{8}m^*\omega_c^2\rho^2+V_{xy}(\rho) \tag{6.1.8}$$

Now it is clear that we can separate two variables, ρ and φ:

$$\phi(\rho,\varphi)=R_{nm}(\rho)\Phi_m(\varphi)=R_{nm}(\rho)e^{im\varphi} \tag{6.1.9}$$

and m should be an integer because the wave function should be unique by a rotation 2π, $\phi_{nm}|_\varphi=\phi_{nm}|_{\varphi+2\pi}$.

$R_{nm}(\rho)$ should satisfy following eigenvalue equation:

$$-\frac{\hbar^2}{2m^*}\left\{\frac{1}{\rho}\frac{\partial}{\partial\rho}(\rho\frac{\partial}{\partial\rho})R_{nm}(\rho)-\frac{m^2}{\rho^2}R_{nm}(\rho)\right\}+\left[\frac{m\hbar\omega_c}{2}+\frac{1}{8}m^*\omega_c^2\rho^2+V_{xy}(\rho)\right]R_{nm}(\rho)=$$

$$= E_{nm} R_{nm}(\rho) \tag{6.1.10}$$

For a special form of in-plane confining potential, a harmonic potential $V_{xy}(\rho) \propto \rho^2$, we have well known analytic solutions of R_{nm}. There are several reasons that this potential is actually realized in vertical quantum dots when the electron number in the dot is very small. So we will only consider the case of harmonic potential. Dimensionally correct form of the potential is:

$$V_{xy}(\rho) = \frac{1}{2} m^* \omega_p^2 \rho^2 \tag{6.1.11}$$

where we introduced a frequency ω_p characterizing the steepness of the confining potential. Typical size of the dot at zero magnetic field is $\sqrt{\hbar/(m^*\omega_p)}$. Therefore the strength of confinement potential effects or determines the size of quantum dot.

First we define another frequency $\Omega = \sqrt{\omega_p^2 + (\omega_c/2)^2}$. Then we define a dimensionless variable $\zeta = \rho^2 m^* \Omega/\hbar$. Since

$$\frac{\partial}{\partial \rho} = \frac{\partial \zeta}{\partial \rho}\frac{\partial}{\partial \zeta} = \frac{2\rho m^* \Omega}{\hbar}\frac{\partial}{\partial \zeta} \tag{6.1.12}$$

Using this expression in equation (6.1.10) we can write:

$$\left[-\frac{\hbar^2}{2m^*}\left\{\frac{1}{\rho}\frac{2\rho m^*\Omega}{\hbar}\frac{\partial}{\partial\zeta}\left(\frac{2\rho m^*\Omega}{\hbar}\right) - \frac{m^2}{\rho^2}\right\} + \frac{1}{8}m^*\omega_c^2\rho^2 + \frac{1}{2}m^*\omega_p^2\rho^2\right] R(\zeta) =$$

$$= \left(E - \frac{m\hbar\omega_c}{2}\right) R(\zeta) \tag{6.1.13}$$

$$-\frac{\hbar^2}{2m^*}\left[\frac{2m^*\Omega}{\hbar}\frac{\partial}{\partial\zeta}(2\zeta\frac{\partial R}{\partial\zeta}) - \frac{m^2}{\rho^2}R\right] + \left(\frac{1}{2}m^*\Omega^2\rho^2 - E + \frac{m\hbar\omega_c}{2}\right) R = 0 \tag{6.1.14}$$

$$-2\hbar\Omega\frac{\partial R}{\partial\zeta} - 2\hbar\Omega\zeta\frac{\partial^2 R}{\partial\zeta^2} + \frac{\hbar^2 m^2}{2m\rho^2}R + \left(\frac{1}{2}m^*\Omega^2\rho^2 - E + \frac{m\hbar\omega_c}{2}\right) R = 0 \tag{6.1.15}$$

You should divide both sides of the above equation by $-2\hbar\Omega$:

$$\zeta\frac{\partial^2 R}{\partial\zeta^2}+\frac{\partial R}{\partial\zeta}+(-\underbrace{\frac{\hbar m^2}{4m\Omega\rho^2}}_{m^2/4\zeta}-\underbrace{\frac{m\Omega\rho^2}{4\hbar}}_{\zeta/4}+\underbrace{\frac{E}{2\hbar\Omega}-\frac{m\omega_c}{4\Omega}}_{\beta})R=0 \tag{6.1.16}$$

where

$$\beta=\frac{E}{2\hbar\Omega}-\frac{m\omega_c}{4\Omega} \tag{6.1.17}$$

$$\zeta\frac{\partial^2 R}{\partial\zeta^2}+\frac{\partial R}{\partial\zeta}+\left(-\frac{\zeta}{4}-\frac{m^2}{4\zeta}+\beta\right)R=0 \tag{6.1.18}$$

In order to solve the equation above in standart form we purpose the solution in terms of a new $X(\zeta)$ function:

$$R(\zeta)=e^{-\zeta/2}\zeta^{|m|/2}X(\zeta) \tag{6.1.19}$$

Then,

$$\frac{\partial R}{\partial\zeta}=X(\zeta)\left[-\frac{1}{2}e^{-\zeta/2}\zeta^{|m|/2}+\frac{|m|}{2}e^{-\zeta/2}\zeta^{|m|/2-1}\right]+e^{-\zeta/2}\zeta^{|m|/2}\frac{\partial X(\zeta)}{\partial\zeta} \tag{6.1.20}$$

$$\frac{\partial R}{\partial\zeta}=\left(-\frac{1}{2}+\frac{|m|}{2\zeta}\right)R(\zeta)+e^{-\zeta/2}\zeta^{|m|/2}\frac{\partial X(\zeta)}{\partial\zeta} \tag{6.1.21}$$

After some arrangements the following expression is found:

$$\zeta\frac{\partial^2 X}{\partial\zeta^2}+(|m|-\zeta+1)\frac{\partial X}{\partial\zeta}+\left(\beta-\frac{|m|}{2}-\frac{1}{2}\right)X=0 \tag{6.1.22}$$

This second order differential equation has special solution: *Kummer confluent-hypergeometric function*

$$X(\zeta)=F[-(\beta-\frac{|m|}{2}-\frac{1}{2}),|m|+1;\zeta] \tag{6.1.23}$$

where $F(\alpha, \gamma, ; z)$ hypergeometric function is defined as:

$$F(\alpha, \gamma, ; z) = \sum_{n=0}^{\infty} \frac{\alpha(\alpha+1)\ldots(\alpha+n-1)z^n}{\gamma(\gamma+1)\ldots(\gamma+n-1)n!} \tag{6.1.24}$$

$$\beta - \frac{|m|}{2} - \frac{1}{2} = n \tag{6.1.25}$$

In the case of negative n values $F[-n, |m|+1; \zeta]$ hypergeometric function has infinity large values. Therefore, $F(-n, |m|+1; \zeta)$ function is reduced to Laguerre polynomial where n is a non-negative integer number.

$$L_n^{(\alpha)}(\zeta) = \frac{\Gamma(\alpha+n+1)}{\Gamma(\alpha+1)n!} F(-n, \alpha+1; \zeta) \tag{6.1.26}$$

Let's insert (6.1.22) and (6.1.17) results into (6.1.25) expression in order to obtain the ground state wave function of an electron confined by parabolic confinement potential in xy plane of a 2D quantum dot as:

$$R(\zeta) = e^{-\zeta/2}\zeta^{|m|/2} L_n^{|m|}(\zeta) \frac{\Gamma(\alpha+1)n!}{\Gamma(\alpha+n+1)} = Ce^{-\zeta/2}\zeta^{|m|/2} L_n^{|m|}(\zeta) \tag{6.1.27}$$

where C is the normalization constant. The solution of Equations (6.1.16) and (6.1.24) gives:

$$n + \frac{|m|}{2} + \frac{1}{2} = \frac{E}{2\hbar\Omega} - \frac{m\omega_c}{4\Omega} \tag{6.1.28}$$

Finally, the energy expression for singe electron in xy plane of a 2D quantum dot is obtained as:

$$E_{n,m} = 2\hbar\Omega \left(n + \frac{|m|}{2} + \frac{1}{2} + \frac{m\omega_c}{4\Omega} \right) \tag{6.1.29}$$

$$E_{n,m} = (2n + |m| + 1)\hbar\Omega + m\frac{\hbar\omega_c}{2} \tag{6.1.30}$$

These energies are known specially as *Fock-Darwin energy spectrum.* The variation of energies versus magnetic field for various n and m values are shown in Figure 6.2.

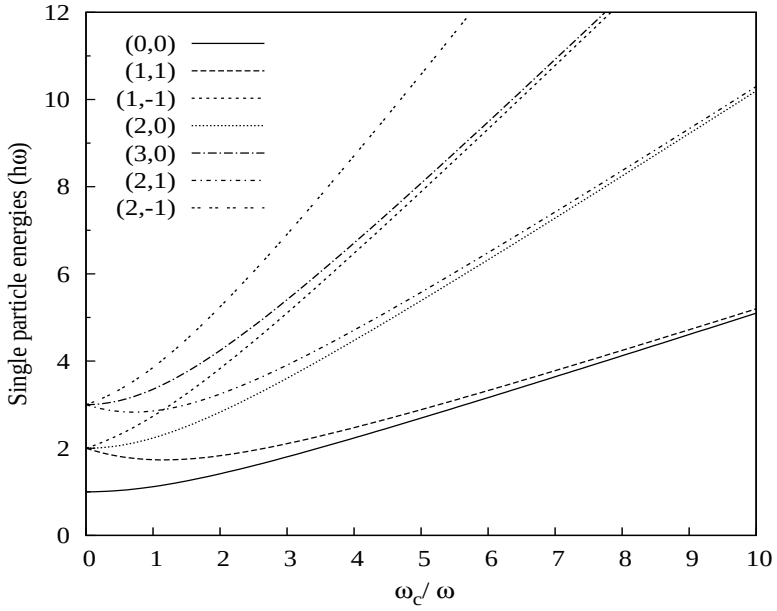

Figure 6.2 Fock Darwin energy spectrum.

Similarly the energy variation in z direction can be defined easily. The confinement potential in the corresponding direction is:

$$V(z) = \begin{cases} 0, & 0 < z < W \\ \infty, & \text{otherwise} \end{cases} \tag{6.1.31}$$

Normalized wave function is:

$$\xi_j(z) = \sqrt{\frac{2}{W}} \sin k_j z \tag{6.1.32}$$

where $k_j = j\pi/W$ and $j = 1, 2, ...$ The eigenenergy of the particle in z direction is well known as:

$$E_j = \frac{\hbar^2}{2m^*} \left(\frac{j\pi}{W}\right)^2 \tag{6.1.33}$$

6.2 Excitons in Parabolic Quantum Dots

6.2.1 Introduction and Motivation

Since the early developments of quantum mechanics, it was immediately recognized that the accurate description of particles correlation is an extremely difficult problem. Since quantum dot (QD) is a gigantic atom with a large but finite number of electrons, it is an interesting model object to study fundamental many-body properties of interacting particles (Bryant, 1988; Garm, 1996; Ikezawa et. al., 2006; Que, 1991; S. Şakiroğlu et. al, 2009; Xie, 2005). An exciton is an electron-hole pair bound by the attractive $-1/r$ Coulomb potential. In quantum dots, binding energies of excitons and excitonic complexes, such as trions and biexcitons, are much larger than those in the bulk materials, and these excitonic complexes strongly influence optical properties of quantum dots (Czajkowski, & Bassani, 1998). In addition to interest of basic physics, these studies are driven by the need for a deep understanding of such confined states for the successful application of quantum structures to quantum information technologies. Large binding energy of the biexciton state is particularly important in light of the recent demonstration of the ability to operate a two-qubit gate using exciton and biexciton states (Ikezawa et. al., 2006; Loss, & DiVincenzo, 1998).

One of the popular and effective methods to deal with particles in semiconductor QDs is the numerical exact diagonalization (Harju, Sverdlov, & Nieminen, 1998; Que, 1991). This method has an intrinsic limitation with respect to the number of particles because of the rapidly growing dimension of matrices under diagonalization and is practically applicable to a QD with around ten electrons (Harju, Sverdlov, & Nieminen, 1998; Maksym, 2005).

An alternative and efficient description can be obtained by using variational

many-body wave function. This old and well-known method to build very accurate solutions of the Schrödinger equation has numerous applications in many fields of physics, such as He-like atoms (Şakiroğlu, Akgüngör, & Sökmen, 2009), the fractional quantum Hall effect (Laughlin, 1983). G. W. Bryant (1988) reported a variational study for ground-state energies and optical properties of excitons in quantum boxes. He used a variational wave function expanded in terms of electron-hole configurations made from electron and hole single-particle box states. Z. Heng & S. Jun-Jie (2004) presented a calculation of the ground state of excitons confined in spherical onion-like quantum-dot quantum-well (QDQW) nanoparticles by using the stochastic variational method with correlated Gaussian bases. G. Bastard *et.al.* (1982) presented a detailed variational calculations for exciton ground state in GaAs-GaAlAs as well as InAs-GaSb quantum well systems. They obtained results for both trial wave functions separable and not separable in spatial coordinates for different well thickness.

The most common way to include correlation into a wave function is to start from the Hartree-Fock picture, and to approximate the exact wave function using Multi-Configuration Self-Consistent Field (MC-SCF) or Configuration Interaction (CI) expansions (Bertini et. al., 1999). Unfortunately, these methods converge very slowly to the exact results.

An alternative approach to study interacting particles in a QD is the explicit inclusion of the interelectronic coordinates into an approximate wave function. James & Coolidge (1933) obtained very good results for two-electron systems by including the interelectronic distance r_{12} into the wave function. Nair, Sinha, & Rustagi (1987) used the variational principle with a three-parameter Hylleraas-type wave function to analyze the quantum size effects on the exciton ground state energies in semiconductor microcrystals. These methods, however, are difficult to generalize for systems with more than two particles since the resulting integrals are extremely difficult or impossible to evaluate analytically.

Quantum Monte Carlo (QMC) methods have become increasingly important tools to study correlated many-body systems. QMC has been successfully applied to find the ground state properties of different systems of interacting particles (Cancio & Chang, 1995; Foulkes et. al., 2001; Harju et. al., 1998; Siljamäki et. al., 2005; Tan, Drummond, & Needs, 2005; Tsuchiya, 2001). Harju *et. al.* (1999) have used Variational Monte Carlo (VMC) method to calculate the ground state energy of up to six electrons in a two dimensional harmonically confined dot and Cancio *et. al.* (1995 to predict confined exciton energy levels in semiconductors. Diffusion QMC within the effective mass approximation (EMA) has been applied by Tsuchiya (2001) to model excitonic complexes in GaAs/AlGaAs quantum wires. Monte Carlo Diagonalization (MCD) method has been used by S. Siljamäki *et.al.* (2005) to study many-electron quantum dot systems, which are either symmetric or perturbed by a point-like charged impurity.

In contrast to numerous studies based on variational approach related to the exciton states in a spherical QD, the variational results reported for excitons in a parabolic QD are still rare. There is certainly a need for methods that are still simple and more accurate.

6.2.2 Theoretical Framework

The total Hamiltonian for the exciton in a parabolic QD can be expressed as:

$$\hat{H} = \sum_{i=\mathrm{e,h}} \left(-\frac{\hbar^2}{2m_i^*}\nabla_i^2 + \frac{1}{2}m_i^*\omega_0^2 r_i^2 \right) - \frac{e^2}{\varepsilon r_{\mathrm{eh}}}, \tag{6.2.1}$$

where m_{e}^* (m_{h}^*), and $\vec{r}_{\mathrm{e}}$ ($\vec{r}_{\mathrm{h}}$) denote the effective mass, and the position vector of the electron (hole), respectively, $r_{\mathrm{eh}} = |\vec{r}_{\mathrm{e}} - \vec{r}_{\mathrm{h}}|$ is the distance between the electron and hole, ω_0 indicates the strength of the confinement, and ε is the dielectric constant of the medium in which the electron and hole are moving. We

consider the GaAs QD with the parabolic confinement potential with the same parabola frequency, w_0, for the electrons and holes. Our calculation is based on effective-mass approximation and ignores the valence band-structure effects. It is convenient to introduce dimensionless variables by following transformations:

$$r_e \to \alpha \tilde{r_e} \qquad\qquad r_h \to \alpha \tilde{r_h} \tag{6.2.2}$$

Here α is parameter in the units of length, and other quantities are dimensionless distances.

$$\hat{H} = -\frac{\hbar^2}{2m_{\mathrm{e}}^*}\frac{1}{\alpha^2}\nabla^2_{\tilde{r_{\mathrm{e}}}} - \frac{\hbar^2}{2m_{\mathrm{h}}^*}\frac{1}{\alpha^2}\nabla^2_{\tilde{r_{\mathrm{h}}}} + \frac{1}{2}m_{\mathrm{e}}^*\omega_0^2\alpha^2\tilde{r_{\mathrm{e}}}^2 + \frac{1}{2}m_{\mathrm{h}}^*\omega_0^2\alpha^2\tilde{r_{\mathrm{h}}}^2 - \frac{e^2}{4\pi\varepsilon_0\varepsilon_r}\frac{1}{\alpha\tilde{r}_{\mathrm{eh}}} \tag{6.2.3}$$

Let's define the following dimensionless parameters:

$$\sigma_{\mathrm{e}} = \frac{m_{\mathrm{e}}^*}{\mu}, \qquad \sigma_{\mathrm{h}} = \frac{m_{\mathrm{h}}^*}{\mu} \tag{6.2.4}$$

where $\mu = \dfrac{m_{\mathrm{e}}^* m_{\mathrm{h}}^*}{m_{\mathrm{e}}^* + m_{\mathrm{h}}^*}$ is the reduced mass of the electron-hole pair. After some arrangements the dimensionless Hamiltonian is obtained as:

$$\tilde{H} = \frac{\hat{H}}{\frac{\hbar^2}{\alpha^2\mu}} = -\frac{1}{2\sigma_e}\nabla^2_{\tilde{r_e}} + \frac{1}{2\sigma_h}\tilde{r_e}^2 - \frac{1}{2\sigma_h}\nabla^2_{\tilde{r_h}} + \frac{1}{2}W^2\sigma_e\tilde{r_e}^2 + \frac{1}{2}W^2\sigma_h\tilde{r_h}^2 - \frac{\kappa}{\tilde{r_{eh}}} \tag{6.2.5}$$

Here W is dimensionless variable defined below and $\tilde{r}_j$ $(j = \mathrm{e}, \mathrm{h}, \mathrm{eh})$ represent dimensionless distances. For simplicity, in what follows we shall use "tildeless" representation of coordinates unless otherwise is stated. The Hamiltonian (6.2.5) contains two length scales: average size of the quantum dot, defined by:

$$R = \sqrt{\hbar/\mu\omega} \tag{6.2.6}$$

and effective Bohr radius,

$$a_B^* = \frac{4\pi\varepsilon\hbar^2}{e^2\mu}. \tag{6.2.7}$$

Then W in Equation (6.2.5) can be written as:

$$W = \left(\frac{a_B^*}{R}\right)^2 \tag{6.2.8}$$

There are also two energy scales. One is the energy quanta due to confinement $\hbar\omega_0$, defined by:

$$\hbar\omega_0 = \frac{\hbar^2}{\mu R^2} \tag{6.2.9}$$

The other energy scale is effective Hartree:

$$E_H^* = \frac{e^4\mu}{(4\pi\varepsilon)^2\hbar^2} = \frac{e^2}{4\pi\varepsilon a_B^*} \tag{6.2.10}$$

The case of $R \ll a_B^*$ describes strong confinement regime and the opposite limit $R \gg a_B^*$ corresponds to weak confinement regime. In the limit case of strong confinement, the effect of Coulomb potential can be neglected and the system acts as harmonic oscillator. Similarly, in the limit of weak confinement, the harmonic potential can be omitted and system have hydrogenic character.

We choose length scale of effective Bohr a_B^* units by setting $\kappa = 1$ and measure energies in effective Hartree E_H^* units. Accordingly the Hamiltonian of the system has the following form:

$$\hat{H} = -\frac{1}{2\sigma_e}\nabla_{r_e}^2 - \frac{1}{2\sigma_h}\nabla_{r_h}^2 + \frac{1}{2}W^2\sigma_e r_e^2 + \frac{1}{2}W^2\sigma_h r_h^2 - \frac{1}{r_{eh}} \tag{6.2.11}$$

To approximate the ground-state wave function for these systems we propose to use a variational trial function of the general form:

$$\Psi_T = \Phi F. \tag{6.2.12}$$

We take the model function Φ, as usual, to be construct from eigenvectors of

single particle Hamiltonian:

$$\Phi(\gamma, r_{\mathrm{e}}, r_{\mathrm{h}}) = \exp\left[-\frac{\gamma}{2} W(\sigma_{\mathrm{e}} r_{\mathrm{e}}^2 + \sigma_{\mathrm{h}} r_{\mathrm{h}}^2)\right], \tag{6.2.13}$$

where γ is a variational parameter. We build the first variational wave function by approximating the correlation function F by a simple exponential with a variational parameter λ

$$F_1(\lambda, r_{\mathrm{eh}}) = \exp(-\lambda r_{\mathrm{eh}}). \tag{6.2.14}$$

We have used the Variational Monte Carlo (VMC) technique for the calculations with $\Psi_1 = \Phi(\gamma, r_{\mathrm{e}}, r_{\mathrm{h}}) F_1(\lambda, r_{\mathrm{eh}})$ trial wave function. The most important gain of using VMC is that it is not restricted to any particular variational form of the wave function. So as function F in Equation (6.2.12), we are free to choose a more suitable functional form than a simple exponential, to get faster convergence.

In this work we also explore the possibility of using different functions of F, in particular the so popular Jastrow term:

$$F_2(a, b, c, r_{\mathrm{eh}}) = J(a, b, c, r_{\mathrm{eh}}) = \exp\left(\frac{a r_{\mathrm{eh}} - b r_{\mathrm{eh}}^2}{1 + c r_{\mathrm{eh}}}\right). \tag{6.2.15}$$

It is not possible to compute analytically the integrals needed to optimize the Jastrow factor, so the optimization of $\Psi_2 = \Phi(\gamma, r_{\mathrm{e}}, r_{\mathrm{h}}) F_2(a, b, c, r_{\mathrm{eh}})$ wave function was done using the VMC method, as explained in the subsection 4.1.

Although the inclusion of the Jastrow factor has been shown to significantly improve the exciton ground-state energies (Cancio, & Chang, 1995; Tan, Drummond, & Needs, 2005) the calculations in this thesis show that it does not always lead to large improvements in the quality of the exciton wave function. In this study we analyze the possibility of inclusion an expansion as a linear combination

of Hylleraas-like coordinates to the exponential correlation functions.

$$F_3(\lambda, r_{\rm e}, r_{\rm h}, r_{\rm eh}) = \exp(-\lambda r_{\rm eh}) \sum_{[n]}^{\mathbb{N}} C_{[n]} r_{\rm e}^{n_e} r_{\rm h}^{n_h} r_{\rm eh}^{n_{\rm eh}}, \tag{6.2.16}$$

$$F_4(a, b, c, r_{\rm e}, r_{\rm h}, r_{\rm eh}) = \exp\left(\frac{a r_{\rm eh} - b r_{\rm eh}^2}{1 + c r_{\rm eh}}\right) \sum_{[n]}^{\mathbb{N}} C_{[n]} r_{\rm e}^{n_e} r_{\rm h}^{n_h} r_{\rm eh}^{n_{eh}}, \tag{6.2.17}$$

where $[n]$ denotes the set of numbers, $[n] = (n_{\rm e}, n_{\rm h}, n_{\rm eh})$. The aim is toward the development of a good correlated basis set. This should keep the number of terms needed to obtain the desired accuracy small, alleviating the problem of the optimization of the nonlinear parameters.

Let set out $N_{\rm e}$, $N_{\rm h}$, $N_{\rm eh}$ the maximum values for $n_{\rm e}$, $n_{\rm h}$, $n_{\rm eh}$ variables, respectively, so that $\mathbb{N} = (N_{\rm e} + 1) \times (N_{\rm h} + 1) \times (N_{\rm eh} + 1)$ gives the size of basis set. The linear expansion parameters, $C_{[n]}$ in Equations (6.2.16) and (6.2.17) have been determined by variational method. Thus the exciton problem reduces to calculating eigenvalues and eigenvectors of the Hamiltonian matrix:

$$\mathbf{KC} = \varepsilon \mathbf{MC} \tag{6.2.18}$$

$\mathbf{C}$ stands for the column matrix of $C_{[n]}$ coefficients. $\mathbf{K}$ and $\mathbf{M}$ are stiffness and mass matrices defined as:

$$\mathbf{K}_{[m],[n]} = \langle \psi_{[m]} | \hat{H} | \psi_{[n]} \rangle = \int \psi^*_{[m]} \left\{ \sum_{i={\rm e,h}} \left(-\frac{1}{2\sigma_i} \nabla_i^2 + \frac{1}{2} W^2 \sigma_i r_i^2 \right) - \frac{1}{r_{\rm eh}} \right\} \psi_{[n]} d\tau_{\rm e} d\tau_{\rm h}, \tag{6.2.19}$$

$$\mathbf{M}_{[m],[n]} = \langle \psi_{[m]} | \psi_{[n]} \rangle = \int \psi^*_{[m]} \psi_{[n]} d\tau_{\rm e} d\tau_{\rm h}, \tag{6.2.20}$$

where $\mathrm{d}\tau_i$ is the volume element either for the electron (e) or the hole (h) and $\psi_{[n]}$ functions are given by:

$$\psi_{[n]} = \Phi F_i r_{\rm e}^{n_e} r_{\rm h}^{n_h} r_{\rm eh}^{n_{eh}} \qquad i = 3, 4. \tag{6.2.21}$$

We obtain the eigenvalues of the random generalized eigenvalue problem [Eq.(6.2.18)] by Monte Carlo Diagonalization method. The matrix elements are calculated by using the Monte Carlo method, as discussed in the following subsection.

6.2.3 Evaluation of matrix elements

Many dimensional integrals of matrix elements are evaluated by implementation of *Correlated sampling Monte Carlo* (CMC) algorithm. The key to the method is the choice of probability distribution function and a simple and efficient algorithm for generating a random series of points $\{\mathbf{R}\}$. The particle coordinates are sampled from the following probability distribution according to the Metropolis algorithm (Metropolis et. al., 1953).

$$P(\gamma, \Lambda, r_{\rm e}, r_{\rm h}, r_{\rm eh}) = N|\psi_{[0]}|^2 = N\left|\exp\left[-\frac{\gamma}{2}W(\sigma_{\rm e}r_{\rm e}^2 + \sigma_{\rm h}r_{\rm h}^2)\right]\exp(-\Lambda r_{\rm eh})\right|^2 \tag{6.2.22}$$

where N is the normalization constant obtained analytically. The variational parameters (Λ, γ) are taken as $\Lambda = \lambda$ for the case of $\Psi_3 = \Phi(\gamma, r_{\rm e}, r_{\rm h})F_3(\lambda, r_{\rm eh})$, while $\gamma = 1$ and $\Lambda = b/c$ for the $\Psi_4 = \Phi(\gamma, r_{\rm e}, r_{\rm h})F_4(a, b, c, r_{\rm eh})$.

K (stiffness) and **M** (mass) matrix elements are defined as:

$$K_{[m],[n]} = \int \psi^*_{[m]}([p], r_e, r_h)\hat{H}\psi_{[n]}([p], r_e, r_h)d\tau_e d\tau_h \tag{6.2.23}$$

$$M_{m,n} = \int \psi^*_{[m]}([p], r_e, r_h)\psi_{[n]}([p], r_e, r_h)d\tau_e d\tau_h \tag{6.2.24}$$

where $[p]$ is the set of variational parameters.

Then, 6.2.23 and 6.2.24 expressions are rewritten as:

$$K_{[m],[n]} = \int \omega_{[m],[n]}([p], r_e, r_h)E_L^{[n]}([p], r_e, r_h)|\psi_{[0]}([p], r_e, r_h)|^2 d\tau \tag{6.2.25}$$

$$M_{[m],[n]} = \int \omega_{[m],[n]}([p], r_e, r_h)|\psi_{[0]}([p], r_e, r_h)|^2 d\tau \tag{6.2.26}$$

where

$$\omega_{[m],[n]}([p], r_e, r_h) = \frac{\psi^*_{[m]}([p], r_e, r_h)\psi_{[n]}([p], r_e, r_h)}{\psi^*_{[0]}([p], r_e, r_h)\psi_{[0]}([p], r_e, r_h)} \tag{6.2.27}$$

is weight function and

$$E_L^{[n]} = \frac{H\psi_{[n]}([p], r_e, r_h)}{\psi_{[n]}([p], r_e, r_h)} \tag{6.2.28}$$

is well known local energy. Correlated sampling Monte Carlo indicate that, $K_{[m],[n]}$'s are mean values $\langle \omega_{[m],[n]} E_L^{\{n\}} \rangle$ taken over $[\mathbf{r_{ei}}, \mathbf{r_{hi}}]$ positions generated randomly with respect to $|\psi_{[0]}|^2$ probability distribution according to any algorithm.

$$K_{[m],[n]} = \lim_{M\to\infty} \frac{\sum_{i=1}^{M} \omega_{[m],[n]}([p], \mathbf{r_{ei}}, \mathbf{r_{hi}}) E_L^{[n]}([p], \mathbf{r_{ei}}, \mathbf{r_{hi}})}{M * N} \tag{6.2.29}$$

Similarly $M_{[m],[n]}$ matrix elements are evaluated over the same distribution function:

$$M_{[m],[n]} = \lim_{M\to\infty} \frac{\sum_{i=1}^{M} \omega_{m,n}([p], \mathbf{r_{ei}}, \mathbf{r_{hi}})}{M * N} \tag{6.2.30}$$

M is Monte Carlo steps and $N = 1/\int |\psi_0([p], r_e, r_h)|^2 d\tau$ is normalization constant obtained analytically (Şakiroğlu, Ph.D. Thesis, 2009).

Finally, given a set of independent points sampled from this distribution, the matrix elements can then be calculated statistically as:

$$K_{[m],[n]} = \langle \omega_{[m][n]} E_{L,[n]} \rangle_{|\psi_{[0]}|^2} \tag{6.2.31}$$

$$M_{[m],[n]} = \langle \omega_{[m][n]} \rangle_{|\psi_{[0]}|^2}, \tag{6.2.32}$$

6.3 Numerical Results and Discussion

A two-particle QD is the simplest nontrivial case of many particle systems. This problem provides a perfect test for QMC since the results of the FEM (Doğan, Ph.D. Thesis, 2009) are available.

Since the extent of the wave function in one direction is much less in the other two, which is the case usually realized in QDs, we assume that electrons move in the plane $r = (x, y)$ under the additional parabolic confinement potential. We present comparative study of variational wave functions for excitons in both 2D disc-like and 3D spherical GaAs QDs and analyze the effect of confinement on exciton ground-state energies.

As noted by Que, (Que, 1992) it can be readly inferred that there are two limiting situations according to the ratio of characteristic length R indicating the size of the QD to the effective Bohr radius a_B^* of the exciton in the bulk material. In the limit $R/a_B^* \gg 1$ the electrons and holes can be thought of as confined independent particles. In this regime, called the strong confinement regime, the Coulomb term turns out to be small with relatively little electron-hole spatial correlation. In the opposite limit, $R/a_B^* \ll 1$ the dominant energy is the Coulomb term. This is the weak confinement situation where the character of the exciton as a quasiparticle is preserved. The limit of the strong confinement is relatively easy to handle. On the other hand, the analysis of the weak confinement limit is rather a difficult task because the uncertainty for the wave function which satisfies the boundary condition (Kayanuma, 1988). According to Kayanuma's report (Kayanuma, 1988) the motional state of the exciton is classified into three regimes: the regime of exciton confinement (weak confinement) for $R/a_B^* \gtrsim 4$, the regime of individual particle confinement (strong confinement) for $R/a_B^* \lesssim 2$, and the intermediate regime for $2 \lesssim R/a_B^* \lesssim 4$. To demonstrate the efficiency of the presented forms of the trial wave functions, we consider several strengths of

the confinement potential in order to describe the weak, intermediate and strong confinement regimes.

VMC energies obtained using the optimized Ψ_1 and Ψ_2 trial wave functions are listed in rows VMC1 and VMC2 of the Tables 6.1 and 6.2, respectively. The results show small differences between the FEM energies and the variational VMC1 values obtained for the weak confinement regime. The difference between the energies increases with R and it is found to be approximately $6 - 7 \times 10^{-3}$ E_H^* in the strong confinement regime. In order to reduce the difference, one must improve the correlation part of the trial wave function. It is clear that the Jastrow factor describes the electron-hole part of the wave function better than the simple exponential. The difference between FEM and variational VMC2 energies is reduced to 2×10^{-3} E_H^* for the strong confinement regime. This result is not unexpected: The Jastrow factor is a generalization of the exponential form, and setting $b = c = 0$, we recover the previous functional form. However, the optimization of the Jastrow term is proved to be much more difficult than the simple exponential.

In order to improve our results we have introduced a serial expansion factor in terms of Hylleraas-like coordinates to the F_1 and F_2 correlation functions. The results obtained from the optimized trial wave functions Ψ_3 and Ψ_4 are shown in the rows MCD1 and MCD2 of the Tables 1 and 2, respectively. We used a basis set of size $\mathbb{N} = 8$ for excitons in both 2D disc-like and 3D spherical parabolic QD's. The superiority of the expanded correlation functions in describing the exciton ground-state energies is obvious from Table 6.1. A relatively small number of terms is sufficient to reach the same level of accuracy in the energy with the similar MCD studies with larger basis set (Siljamäki et. al., 2005). The MCD1 energies are in good agreement with the previous variational calculations reported for the same system, carried analytically using Ψ_3 trial wave function, (Şakiroğlu et.al., 2009) provided that a careful optimization is performed. On the other

Table 6.1 FEM and QMC results for ground state energies of an exciton in 3D spherical parabolic QD as a function of the QD radius R, normalized by the bulk exciton Bohr radius a_B^*. Energies are in E_H^* units. The statistical error in the last digit is in the parentheses.

R/a_B^*	VMC1	MCD1	VMC2	MCD2	FEM
5.774	-0.45296(2)	-0.4532(3)	-0.45263(1)	-0.4537(3)	-0.453642
5.000	-0.43721(2)	-0.4372(2)	-0.43724(2)	-0.4374(2)	-0.437619
4.082	-0.40390(3)	-0.4043(2)	-0.40425(2)	-0.4041(2)	-0.404697
3.015	-0.316085(8)	-0.3168(2)	-0.31684(3)	-0.3170(2)	-0.317815
2.085	-0.08481(2)	-0.0862(3)	-0.08641(1)	-0.0873(2)	-0.088213
1.374	0.56639(2)	0.5640(4)	0.56364(3)	0.5622(4)	0.561299
0.985	1.75946(4)	1.7568(2)	1.75560(2)	1.7543(3)	1.753454
0.808	3.01556(3)	3.0128(3)	3.01172(3)	3.0105(3)	3.009859
0.702	4.30770(3)	4.3052(4)	4.30366(2)	4.3029(4)	4.301980
0.629	5.62342(4)	5.6207(5)	5.61915(3)	5.6177(5)	5.617631
0.532	8.30183(4)	8.2989(6)	8.29725(3)	8.2957(6)	8.295962
0.498	9.65797(4)	9.6548(6)	9.65327(3)	9.6520(8)	9.652032
0.470	11.02264(4)	11.0199(7)	11.01774(3)	11.0167(8)	11.016641
0.446	12.39440(4)	12.3914(8)	12.38950(3)	12.3886(9)	12.388431
0.425	13.77221(5)	13.7690(9)	13.76735(3)	13.766(1)	13.766369

hand, a single optimized Jastrow correlation factor, has recovered more of the FEM energies with respect to F_3 correlation function. The MCD1 energies could be improved by including more terms, at the expense, of course, of a larger basis set. We do not see any deviations of MCD2 energies from the FEM results for the weak as well as the strong confinement regimes within the statistical error, while there is approximately $1 \times 10^{-3} E_H^*$ difference for the intermediate regime, and this demonstrates the good quality of our ansatz. Thus we conclude that the improved variational function Ψ_4 is able to capture nearly exactly the exciton ground state energy in 3D spherical GaAs QDs.

The ground state energies for the 2D exciton obtained using $\Psi_1 - \Psi_4$ trial wave functions, described above, are shown as a function of normalized QD radius in Table 6.2.

The results suggest that all the proposed trial wave functions give almost the same ground state energies in weak confinement regime. It is similar for 2D disc-like QDs, that the optimized Ψ_2 trial wave functions improve VMC1 energies especially in strong confinement regime. The difference between the energies is approximately $0.01 - 0.02 E_H^*$. The MCD method has been tested for exciton ground-state energies in GaAs quantum disc with variational calculations carried analytically using Ψ_3 trial wave function with the same basis set (Şakiroğlu et.al., 2009) to show excellent performance. On the other hand, our MCD2 results do not show any deviations from the VMC2 energies within the statistical error. Furthermore, as R increases, the exciton ground-state energy approaches the energy of the unconfined two-dimensional exciton ($-2.0 E_H^*$).

One can see that the variances in the MCD energies are greater than VMC, which is an expected result, because the statistical errors of all matrix elements are correlated.

Table 6.2 QMC ground state energies in E_H^* units for an exciton in quantum disc obtained from the trial functions $\Psi_1 - \Psi_4$ as a function of the QD radius R, normalized by the bulk exciton Bohr radius a_B^*. The statistical error in the last digit is in the parentheses.

R/a_B^*	VMC1	MCD1	VMC2	MCD2
5.774	-1.969764(7)	-1.9691(10)	-1.969805(8)	-1.9697(9)
5.000	-1.95960(1)	-1.959(1)	-1.9596995(9)	-1.960(1)
4.082	-1.93912(1)	-1.9389(10)	-1.9393254(3)	-1.939(2)
3.015	-1.88706(1)	-1.887(1)	-1.8877368(7)	-1.887(2)
2.085	-1.75798(4)	-1.758(1)	-1.760182(3)	-1.760(2)
1.374	-1.41234(9)	-1.4144(8)	-1.41889(1)	-1.419(1)
0.985	-0.76877(5)	-0.7857(9)	-0.79573(2)	-0.796(1)
0.702	0.6079(2)	0.5983(10)	0.58513(2)	0.585(1)
0.629	1.3438(2)	1.332(1)	1.31969(2)	1.319(1)
0.532	2.8715(2)	2.861(1)	2.84628(2)	2.846(1)
0.498	3.6581(2)	3.647(1)	3.63140(2)	3.631(1)
0.470	4.4557(2)	4.443(1)	4.42801(2)	4.427(1)
0.446	5.2630(2)	5.249(1)	5.23444(2)	5.233(1)
0.425	6.0784(2)	6.064(1)	6.04941(2)	6.049(1)

Note that, in small QD's exciton energy is sensitive to QD radius. For small R, the dominant effect of parabolic confinement gives rise to increase of exciton energy. In larger QD's exciton confinement strength decays and exciton behavior

begins to resemble that of bulk. The similar variation has been reported by Garm (Garm, 1996) for spherical parabolic GaAs quantum dots. The exciton ground energy states in 2D disc like QD's are significantly lower than the corresponding states in 3D spherical parabolic QD.

6.3.1 Exciton Binding Energies

The difference between the exciton energy and the sum of the single-particle energies is commonly called the binding energy:

$$E_b = E_{\mathrm{e}} + E_{\mathrm{h}} - E_X \tag{6.3.1}$$

E_X is the ground state energy of the exciton, E_{e} and E_{h} are the energies of an uncorrelated electron and hole in the QD, respectively. The binding energy as a function of QD radius R, normalized by the bulk exciton Bohr radius a_B^* is plotted for 2D disc like and 3D spherical parabolic QD's in Figure 6.3. MCD2 energy values have been used as E_X in binding energy calculations for both cases. As expected, the binding energy is found to increase with enhancing the spatial confinement; this is in agreement with the results obtained previously in quantum dots (Que, 1992; Xie, 2005). This is due to decreasing dot radius and consequently increase in the spatial overlap between an electron and hole. The high binding energies obtained in 2D QD's show that the excitons are more stable in these systems.

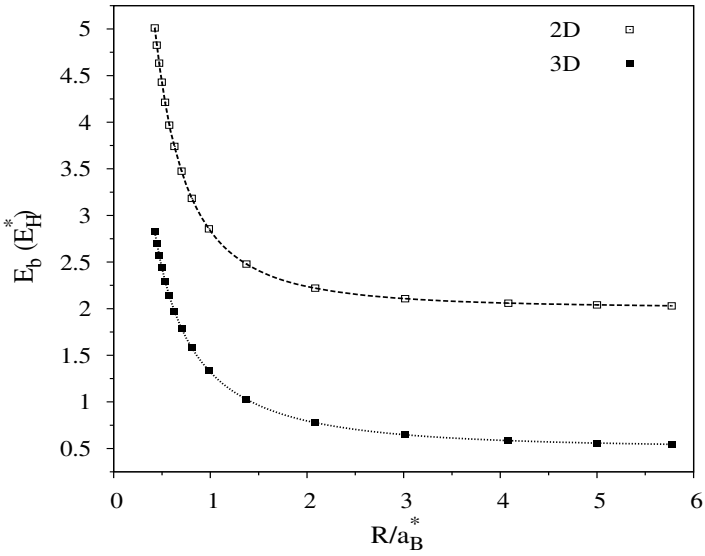

Figure 6.3 The exciton binding energies in GaAs quantum dots as a function of the QD radius R, normalized by the bulk exciton Bohr radius a_B^*. Statistical errors are smaller than symbols indicating numerical data.

6.4 Ground State Energies of Two-Electrons in Parabolic Quantum Dots

6.4.1 Introduction and Motivation

The experimental realization of quantum dots has stimulated great theoretical efforts towards interpretation of their various physical properties arising from the reduced dimensionality. The relative strength of electron-electron and electron-confinement interaction can be experimentally tuned over a wide range resulting in a peculiar electronic system with tunable physical properties. For this reason, quantum dots are sometimes referred to as "artificial atoms". In a typical quantum dot, all electrons are tightly bound, except for a few free electrons. Such artificial atoms are of immense technological value because they form the building units of larger structures. Quantum dots can contain anything

from a single electron to a collection of thousands of electrons and much of the parameters that describe a quantum dot can be precisely controlled by conventional nanofabrication methods. The two-electron system is sometimes called quantum dot helium (Pfannkuche, & Gerhardts, 1993) and is the simplest example of electron correlation in quantum dots. It has been studied extensively by exact-diagonalization (Merkt, Huser & Wagner, 1991; Ciftja, & Kumar, 2004), Hartree-Fock (Johnson, & Reina, 1992), analytic approximation methods (González, Quiroga, & Rodriguez, 1996; El-Said, 1996; Taut, 1994) as well as QMC methods (Bolton, 1996; Harju, Siljamäki, & Nieminen, 2002; Pederiva, Umrigar, & Lipparini, 2000).

In this work, we study the ground-state properties of 2D and 3D quantum-dot helium in zero external magnetic field by using Variational Monte Carlo and Monte Carlo Diagonalization methods. The two approaches will serve as a testing ground to build high-quality trial wave functions for quantum dot systems with arbitrary number N of electrons. Given that a good variational wave function itself can be an excellent approximation to the true exact ground state, there is always a need to find better, yet simple enough ways to accurately describe such complicated systems as the quantum dots. The main motivation of the present work is to identify and demonstrate that a variational wave function with a Hylleraas-like expansion different from those previously considered in the literature constitutes the best choice to describe the ground state of this system.

6.4.2 Theoretical Framework

The system of two interacting electrons of m^* effective mass confined in a quantum dot by parabolic potential is described by the Hamiltonian:

$$\hat{H} = \sum_{i=1}^{2} \left(-\frac{\hbar^2}{2m^*}\nabla_i^2 + \frac{1}{2}m_i^*\omega_0^2 r_i^2 \right) + \frac{e^2}{4\pi\varepsilon r_{12}} \tag{6.4.1}$$

Here ω_0 is the confining frequency and ε_0 is the dielectric constant of the medium in which the electrons are moving. The position vector of each electron is denoted by r_i $(i = 1, 2)$, and r_{12} is the interelectronic distance. There are two length scales related to the problem: the effective Bohr radius a_B^*, and the characteristic quantum dot size R:

$$a_B^* = \frac{4\pi\varepsilon\hbar^2}{m^* e^2} \qquad R = \sqrt{\frac{\hbar}{m^*\omega_0}} \tag{6.4.2}$$

We use length scale of a_B^* and measure energies in units of effective Hartree $E_{\mathrm{H}}^* = m^* e^4/\hbar^2(4\pi\varepsilon)^2$. The resulting dimensionless Hamiltonian is:

$$\hat{H} = \sum_{i=1}^{2}\left(-\frac{1}{2}\nabla_i^2 + \frac{1}{2}W^2 r_i^2\right) + \frac{1}{r_{12}} \tag{6.4.3}$$

where dimensionless variable $W = (a_B^*/R)^2$ describes the strength of the confinement energy relative to the Coulomb energy.

Among different quantities describing a quantum dot, the study of the ground-state properties is of fundamental importance, therefore we focus our main interest on the ground-state wave function and the ground-state energy. Even in the case of 2D quantum-dot helium in zero magnetic field, an exact analytic solution of the problem is not available, therefore most of the methods used so far, rely on approximations or numerical calculations that some time differ considerably with each other.

We perform the variational quantum Monte Carlo techniques to study two electrons in a parabolic quantum dot by using the trial wave function of the general form:

$$\Psi_T = \Phi F \tag{6.4.4}$$

as in the case of excitons in the corresponding systems. Similarly, Φ function is given by:

$$\Phi(\gamma, r_1, r_2) = \exp\left[-\frac{\gamma}{2}W(r_1^2 + r_2^2)\right] \tag{6.4.5}$$

and correspond to the product of the exact ground state wave functions of uncorrelated electrons in parabolic confinement with strength W. Here γ is the variational parameter. F is the important correlation part of the trial wave function, which should describe the correlations between electrons correctly as possible.

We start by consider Jastrow factor as correlation function given by:

$$F_1(a, b, c, r_{12}) = \exp\left(\frac{ar_{12} - br_{12}}{1 + cr_{12}}\right) \tag{6.4.6}$$

where a, b and c are positive variational parameters to be optimized. Using the VMC algorithm the expectation value of the energy for the trial wavefunction $\Psi_1([p], r_1, r_2, r_{12}) = \Phi(\gamma, r_1, r_2)F_1(a, b, c, r_{12})$ can be estimated by averaging the local energy $E_{\mathrm{L}} = \hat{H}\Psi_1/\Psi_1$ over an ensemble of configurations distributed as $|\Psi_1|^2$, sampled during a random walk in the configuration space using Metropolis algorithm:

$$E[\Psi_1] = \frac{\int \Psi_1^2([p], r_1, r_2, r_{12})E_{\mathrm{L}}([p], r_1, r_2, r_{12})d\Omega_1 d\Omega_2}{\int \Psi_1^2([p], r_1, r_2, r_{12})d\Omega_1 d\Omega_2} = \langle E_L \rangle_{|\Psi_1|^2} \tag{6.4.7}$$

Here $[p]$ denotes the variational parameters group consist of a, b, c and we consider $\gamma = 1$. The possible fluctuations of the local energy due to Coulomb singularities, which strongly influence the convergence numerical results, were suppressed by electron-electron cusp conditions. The cusp condition is adressed by $a = 2$ for 2D disc-like QD and $a = 1$ in the case of 3D spherical parabolic QD. These parameters were optimized according to energy minimization criteria.

We construct the second, $\Psi_2 = \Phi(\gamma, r_1, r_2)F_2(\lambda, r_{12})$, and third trial wave functions, $\Psi_3 = \Phi(\gamma, r_1, r_2)F_3(a, b, c, r_{12})$, such that the correlation parts involve

expansion in terms of Hylleraas-like coordinates written in the following forms:

$$F_2(\lambda, r_1, r_2, r_{12}) = \exp(-\lambda r_{12}) \sum_{[n]}^{N} C_{[n]} r_1^{n_1} r_2^{n_2} r_{12}^{n_{12}} \tag{6.4.8}$$

$$F_3(a, b, c, r_1, r_2, r_{12}) = \exp\left(\frac{a r_{12} - b r_{12}^2}{1 + c r_{12}}\right) \sum_{[n]}^{N} C_{[n]} r_1^{n_1} r_2^{n_2} r_{12}^{n_{12}} \tag{6.4.9}$$

where $[n]$ denotes the set of numbers $[n] = (n_1, n_2, n_{12})$. N_1, N_2, and N_{12} are the maximum values of n_1, n_2, and n_{12} variables, respectively, so that $N = (N_1 + 1) \times (N_2 + 1) \times (N_{12} + 1)$ defines the size of basis set. The optimization of C_n linear expansion parameters according to variational principle reduces the problem to generalized eigenvalue equation as shown in chapter 4.2.

$$\mathbf{KC} = \varepsilon \mathbf{MC} \tag{6.4.10}$$

$\mathbf{C}$ is the column matrix of $C_{[n]}$ coefficients. $\mathbf{K}$ and $\mathbf{M}$ are stiffness and mass matrices defined as:

$$\mathbf{K}_{[m],[n]} = \langle \psi_{[m]} | \hat{H} | \psi_{[n]} \rangle = \int \psi^*_{[m]} \left\{ \sum_{i=1,2} \left(-\frac{1}{2}\nabla_i^2 + \frac{1}{2} W^2 r_i^2 \right) + \frac{1}{r_{12}} \right\} \psi_{[n]} d\Omega_1 d\Omega_2, \tag{6.4.11}$$

$$\mathbf{M}_{[m],[n]} = \langle \psi_{[m]} | \psi_{[n]} \rangle = \int \psi^*_{[m]} \psi_{[n]} d\Omega_1 d\Omega_2, \tag{6.4.12}$$

where $\mathrm{d}\Omega_i, (i = 1, 2)$ are the volume elements for each electron and $\psi_{[n]}$ functions are given by:

$$\psi_{[n]} = \Phi F_i r_1^{n_1} r_2^{n_2} r_{12}^{n_{12}} \qquad i = 2, 3. \tag{6.4.13}$$

These matrix elements are evaluated in the same way as described in subsection 6.3.1. We used a basis set of size $\mathbb{N} = 8$ for electrons in both 2D disc-like and 3D spherical parabolic QD's.

6.4.3 Numerical Results and Discussion

The dimensionless ground state energies, $E/E^*_{\rm H}$, for 3D and 2D quantum dot helium systems for values of W from 0.05 to 10 are listed in Tables 6.3 and 6.4, respectively. The optimal value of parameter γ of Ψ_2 variational wave function was found to varies in the range of $0.86-1.0$, and the parameter λ to changes in the interval $0.01-0.25$ for all W's under consideration in the case of 3D quantum dot. In a similar way, the optimal parameter γ is found be in the range of $0.76-1.0$, and the optimal λ to vary as $0.01-0.3$ in the 2D quantum dot. Furthermore the optimal parameter c is found to be in the range of $0.6-2.3$ of both Ψ_1 and Ψ_3 variational wave functions for 3D and $0.2-2.8$ for 2D quantum dot systems. On the other hand, the results show that the parameter b, $(0.001 < b < 0.01)$, do not have a decisive effect on ground sate energies of 2D as well as 3D quantum dot helium systems.

The results clearly show that second optimized wave function, Ψ_2, is the best choice to study 2D as well as 3D quantum dot helium systems. MCD1 energies are quantitatively identical with data in Ref. Şakiroğlu et. al., (2009) obtained from similar basis set by introducing integral transforms for the terms as $r_{12}^k \exp(-\lambda r_{12})$ which enable to calculate the relevant matrix elements analytically.

The inclusion of the serial expansion in terms of Hylleraas-like coordinates improves the ground state energies of 2D as well as 3D quantum dot helium systems, which is an expected result. However, the expansion term combined with the simple exponential form, $\exp(-\lambda r_{12})$, describes the relevant system better than the same expansion multiplied by the Jastrow factor. Ineffectiveness of parameter b contributes to this result. On the other hand, the previous calculations for the excitons confined in parabolic QDs, show that the correlation function, $F_4 = J(a,b,c,r_{\rm eh})\sum_{[n]} C_{[n]} r_{\rm e}^{n_{\rm e}} r_{\rm h}^{n_{\rm h}} r_{\rm eh}^{n_{\rm eh}}$, is the best choice.

Table 6.3 QMC ground state energies in E_H^* units for interacting two electrons in 3D quantum dot obtained from the trial functions $\Psi_1 - \Psi_3$ as a function of W. The statistical error in the last digit is in the parentheses.

W	VMC	MCD1	MCD2
0.05	0.28505(1)	0.28295(4)	0.28338(7)
1.0	3.7338(1)	3.7301(3)	3.7317(3)
		3.7301[a]	
2.0	7.0614(2)	7.0579(6)	7.0602(5)
		7.05785[a]	
4.0	13.5270(3)	13.522(1)	13.5256(8)
		13.5232[a]	
6.0	19.8848(3)	19.878(1)	19.882(1)
8.0	26.1867(3)	26.181(2)	26.184(1)
10.0	32.4530(3)	32.448(2)	32.450(1)
		32.44865[a]	

[a]Ref. Şakiroğlu et. al. (2009)

Another important conclusion seen from Tables 6.3 and 6.4 is that the energies enhance as the dimensionality of the quantum dot increases.

To demonstrate the efficiency of our method with respect to the QD dimensionality and to investigate the details of size effect, it is interesting to study the electron-electron interaction energies, $E_{\mathrm{e-e}} = \langle 1/r_{12} \rangle$. The electron-electron

Table 6.4 QMC ground state energies in E_H^* units for interacting two electrons in quantum disc obtained from the trial functions $\Psi_1 - \Psi_3$ as a function of W. The statistical error in the last digit is in the parentheses.

W	VMC	MCD1	MCD2
0.05	0.257432(8)	0.25861(6)	0.2552(2)
1.0	3.0134(3)	3.0001(4)	3.0070(4)
		3.0000[a]	
2.0	5.5136(4)	5.4964(6)	5.5058(6)
		5.4965[a]	
4.0	10.233(1)	10.212(1)	10.2233(9)
		10.2126[a]	
6.0	14.789(1)	14.766(2)	14.778(1)
8.0	19.260(1)	19.236(2)	19.249(1)
10.0	23.676(1)	23.650(2)	23.664(2)
		23.65165[a]	

[a]Ref. Şakiroğlu et. al. (2009)

interaction energies, calculated at particular confinement frequency W, may be obtained simply by substituting out the energies of noninteracting electrons in parabolic potential from the total energy of the system.

In Figures 6.4 and 6.5 we plot the ground state energies together with one-electron and Coulomb energy contributions as a function of W correlation parameter for 3D and 2D QD helium, respectively. It is clear that the sum

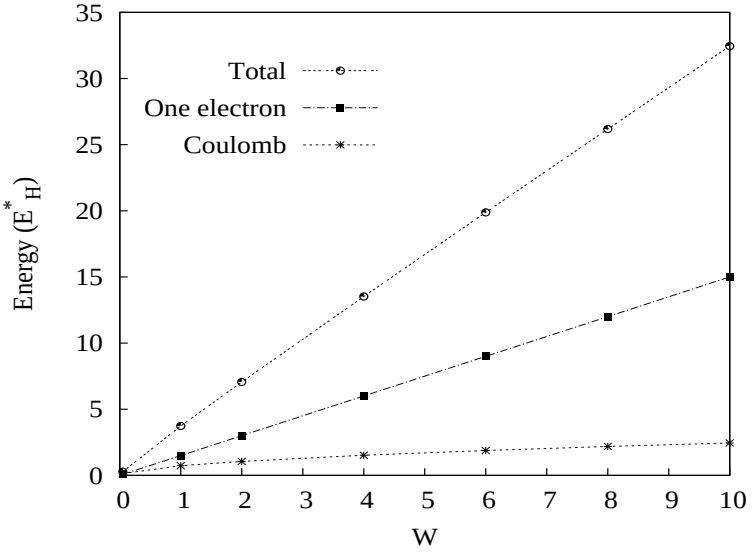

Figure 6.4 Ground state energy together with one-electron and Coulomb contributions of two electrons confined in 3D parabolic quantum dot as a function of W correlation parameter. Statistical errors are smaller than symbols indicating numerical data.

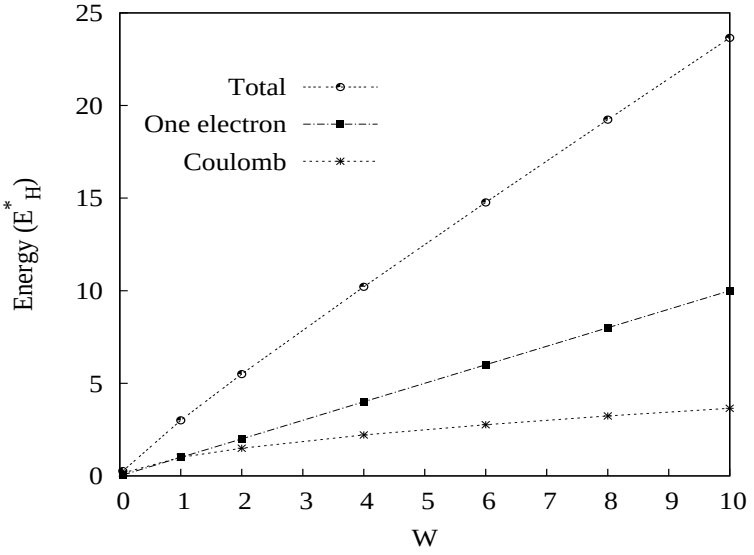

Figure 6.5 Ground state energy together with one-electron and Coulomb contributions of two electrons confined in 2D parabolic quantum disc as a function of W correlation parameter. Statistical errors are smaller than symbols indicating numerical data.

of single electron energies are the dominant component of the total ground state energy in both cases. These graphs are also in good agreement with the energies predicted by the calculations done in Ref. (El-Said, 2002).

In addition to this, as the confinement strength strongly increases, i.e. $W \longrightarrow \infty$, the energy values approach to the exact results of the harmonic oscillator energies: E/W = 2.0 and 3.0, in 2D and 3D, respectively. Thus we can say that our method and variational wavefunction is applicable to the entire range of W.

CHAPTER SEVEN
CONCLUSION

In this thesis the ground-state energies of the interacting two-electrons and electron-hole pair in two dimensional disc-like and three dimensional spherical parabolic quantum dots are calculated via QMC methods, using a sequence of four variational wave functions. The variational wave functions are the product of a noninteracting harmonic-oscillator wave function for the single particles and a pair correlation function of the separation between the particles. For variational wave functions with simple exponential, $\exp(-\lambda r_{ij})$, or Jastrow form, which include the two lowest powers of particles separation, r_{ij}, the ground state energies were evaluated using the Variational Monte Carlo method, whereas for variational wave functions with higher powers of r_{ij} appearing in Hylleraas-like form in correlation functions, the ground-state energies were calculated using the Monte Carlo Diagonalization method.

Good agreement was found between the results obtained for variational wave functions with Jastrow factor multiplied by Hylleraas-like expansion and exciton ground-state energies obtained using finite element method. This consistency indicates that this optimal wave function is a good choice to study excitons confined in 2D and 3D quantum dots of different sizes. The binding energies calculated from these results show that excitons are more stable in two-dimensional quantum dots.

To assess the capabilities of the proposed ansatzs we also tested these variational wave functions for two interacting electrons confined in parabolic quantum dots. The results show that the correlation function constructed as product of simple exponential form and Hylleraas expansion describes electron-electron correlations more properly comparing to the other suggested wave functions for both 2D and 3D quantum dots.

The optimization of variational parameters is crucial in VMC as well as MCD methods. Comparison with previous analytical and numerical studies indicate that a careful optimization is performed. Very few terms are needed to reach an accuracy comparable to more common wave function forms with large basis sets. The numerical technique puts no constraints on the potential and can be systematically improved by adding more terms using the procedure described.

In conclusion it has been seen that the MCD method via proposed variational function in terms of Hylleraas-like expansion provides an easy and efficient tool to study the ground-state energies of two interacting particles confined in parabolic quantum dots and enables to treat the particle-particle correlations correctly.

It should also be suggested that these WF's could be tested for quantum dots with varying number of confined electrons. Usually it is not easy to obtain analytical result for integrals of matrix elements. In the MCD method, the matrices are evaluated statistically, and there are no restrictions on the basis functions at all. In the case of any changes in Hamiltonian or basis functions matrix elements do not need to be regenerated, unlike the Exact Diagonalization method. It should be simple enough to make any changes in the corresponding system and to implement calculations for larger number of particles feasible.

Another easy and natural extension to the current program is to parallelize the code. The above extensions would result in a very efficient tool for many-body quantum mechanics, that can be applied to a wide variety of problems. An interesting applications could be to apply the MCD method to Density Functional Theory (DFT) determinants for large systems.

REFERENCES

Bryant, G. W. (1988). Excitons in quantum boxes: Correlation effects and quantum confinement. *Physical Review B*, *37*, 8763.

Bastard, G., Mendez, E. E., Chang, L. L., & Esaki L. (1982). Exciton binding energy in quantum wells. *Physical Review B*, *26*, 1974.

Bertini, L., Bressanini, D., Mella, M., & Morosi, G. (1999). Linear expansions of correlated functions: Variational Monte Carlo case study. *International Journal of Quantum Chemistry*, *74*, 23.

Brunner, R., Meisels, R., Kuchar, F., ElHassan, M., Bird, J., & Ishibashi, K. (2004). Investigations of backscattering peaks and of the nature of the confining potential in open quantum dots. *Physica E*, *21*, 491.

Borovitskaya, E., & Shur, M. S. (2002). *Quantum Dots*. Brooklyn: World Scientific Publishing Company.

Bolton, F. (1996). Fixed-phase quantum Monte Carlo method applied to interacting electrons in a quantum dot. *Physical Review B*, *54*, 4780.

Czajkowski, G., & Bassani, F. (1972). Optical properties of excitons in low dimensional systems. *Physica Status Solidi (a)*, *170*, 249.

Cancio, A., & Chang, Y. (1995). Polyexcitons and bound multiple excitons in semiconductors studied by quantum Monte Carlo methods. *Chinese Journal of Physics*, *33*, 335.

Ceperley, D., Chester G., V., & Kalos, M. H. (1977). Monte Carlo simulation of a many-fermion study. *Physical Review B*, *16*, 3081.

Ciftja, O., & Faruk, M. G. (2007). Two-dimensional quantum dot helium in a magnetic field: variational theory. arXiv: 0708.3690v1.

D'Andrea, A., Del Sole, R., & Cho, K. (1990). Exciton Quantization in CdTe Thin Films. *Europhysics Letters*, *11*, 169.

Deak Lam Ltd. (n.d). *Future Technology.* Retrieved 10 July, 2009, from http://deak-lam.com/index_files/Page1141.htm

Doran, J. P., Donegan, J. F., Hegarty, J., Feldman, R. D., & Austin, R. F. (1992). Quantum well width dependence of exciton-phonon interaction in $Cd_{0.33}Zn_{0.67}Te$/ZnTe single quantum wells. *Solid State Communications*, *81*, 801.

Doğan Ü. (2009). *M*esh generation and electronic structure of quantum wires. İzmir Ph.D. Thesis (unpublished).

Drakos, N. (1995). *Introduction to Monte Carlo Methods*, (5.th edition). USA: Computer Based Learning Unit, University of Leeds.

Efros, Al. L., & Efros, A. L. (1982). *Soviet Phys. Semicond.*, *20*, 808.

Ekimov, A. I., & Onuschenko, A. A. (1981). Quantum Size Effect in 3-Dimensional Microscopic Semiconductor Crystals. *JETP Letters*, *34*, 345., (1984), *Ibid. 40*, 1136.

El-Said, M. (1992). The ground-state energy of an exciton in a parabolic quantum dot. *Semicond. Sci. Technol.*, *9*, 272.

El-Said, M. (2002). The spectral properties of two interacting electrons in a quantum dot. *Turkish Journal of Physics*, *2*6, 331.

Einevoll, G. T. (1992). Confinement of excitons in quantum dots. *Physical Review B*, *45*, 3410.

Foulkes, W. M. C., Mitas, L., Needs, R. J., & Rajagopal, G. (2001). Quantum Monte Carlo simulations of solids. *Review of Modern Physics*, *73*, 33.

Ferguson, D. M., Siepmann, J. I., & Truhlar, D. G. (1998). *Monte Carlo methods in Chemical Physics*. (1st. edition). USA: Wiley-Interscience.

Greene, R. L., & Bajaj, K. K. (1983). Binding energies of wannier excitons in $GaAs-Ga_{1-x}Al_xAs$ quantum well structures. *Solid State Communications*, *45*, 831.

Garm, T. J. (1996). Exciton states in spherical parabolic GaAs quantum dots. *Journal of Physics: Condensed Matter*, *8*, 5725.

Geerinckx, F., Peeters, F. M., & Devreese, J. T. (1990). Effect of the confining potential on the magneto-optical spectrum of a quantum dot. *Journal of Applied Physics*, *68*, 3435.

Gaudoin, R. (1999). *Correlated many-electron wavefunctions for quantum Monte Carlo calculations of strongly inhomogeneous systems*. London: Ph.D. Thesis

González, A., Quiroga, L., & Rodriguez, B. A. (1996). Planar three-body problem with Calogero interactions and a magnetic field. *Few-Body Systems*, *21*, 47.

Harju, A., Sverdlov, V. A., & Nieminen, R. M. (1998). Variational wave function for a quantum dot in a magnetic field: A quantum Monte Carlo study. *Europhysics Letters*, *41*, 407.

Harju, A., Sverdlov, V. A., Nieminen, R. M. & Halonen, V. (1999). Many-body wave function for a quantum dot in a weak magnetic field. *Physical Review B*, *59*, 5622.

Harju, A., Siljamäki, S., & Nieminen, R. M. (2002). Wigner molecules in quantum dots: A quantum Monte Carlo study. *Physical Review B*, *59*, 5622.

Heng, Z., & Jun-Jie, S. (2004). Ground state of excitons in quantum-dot quantum-well nanoparticles: stochastic variational method. *Chinese Physics 13*, 2136.

Huffaker, D. L., Park G., Zou Z., Shchekin, O. B., & Deppe D. G. (1998). 1.3μm room-temperature GaAs-based quantum dot laser. *Applied Physics Letters*, *73*, 2564.

Hutton, D. V. (2004). *Fundamentals of finite element analysis*. New York: McGraw-Hill.

Hammond, B. L., Lester, Jr. W. A., & Reynolds, P. J. (1994). *Monte Carlo methods in ab initio quantum chemistry*. Singapore: World Scientific Publishing.

Helle, M. (2006). *Few-Electron Quantum Dot Molecules*. Helsinki: Ph.D. Thessis.

Ikezawa, M., Nair, S. V., Ren, H., Masumoto, Y., & Ruda, H. (2006). Biexciton binding energy in parabolic GaAs quantum dots. *Physical Review B*, *73*, 125321.

James, H. M., & Coolidge, A. S. (1933). The ground state of the hydrogen molecule. *Journal of Chemical Physics*, *1*, 825.

Jaziri, S., Bennaceur, R. (1994). Excitons in parabolic quantum dots in electric and magnetic fields. *Semicond. Sci. Technol.*, *9*, 1775-1781.

Jiawei, L., Zhizhen, Y. & Nasser, N. M. (2003). GaN-based quantum dots. *Physica E*, *16*, 244.

Johnson, N. F., & Reina M. (1992). *The accuracy of Hartree-Fock approximation for quantum dots. Journal of Physics: Condensed Matter*, *4*, L623.

James, A. J. (1995). *Solving the many electron problem with quantum Monte-Carlo methods*. London: Ph.D. Thesis.

Kayanuma, Y. (1988). Quantum-size effects of interacting electrons and holes in semiconductor mycrocrystals with spherical shape. *Physical Review B*, *38*, 9797.

Knuuttila, L. (2006). *Growth and properties of compound semiconductors on germanium substrate*. Helsinki: Ph.D. Thesis.

Ciftja, O., & Kumar, A. (2004). Ground State of two-dimensional quantum-dot helium in zero magnetic field: Perturbation, diagonalization, and variational theory. *Physical Review B*, *70*, 205326.

Kumar, A., Laux, S. E., & Stern, F. (1990). Electron states in a GaAs quantum dot in a magnetic field. *Physical Review B*, *42*, 5166.

Kouwenhoven, L. P., Austing, D. G., & Tarucha, S. (2001). Few-electron Quantum Dots. *Report on Progress in Physics*, *64*, 701-736.

Kent, P. R. C. (1999). *Techniques and applications of quantum Monte Carlo*. Cambridge: Ph.D. Thesis.

Loss, D., & DiVincenzo, D. P. (1998). Quantum computation with quantum dots. *Physical Review A*, *57*, 120.

Laughlin, R. B. (1983). Anomalous quantum hall effect: An incompressible quantum fluid with fractionally charged excitations. *Physical Review Letters*, *50*, 1395.

Maksym, P. A. (2005). Auxiliary field quantum Monte-Carlo simulation of interacting electrons in quantum dots. *Physica E*, *26*, 257.

Masumoto, Y., Takagahara, T. (2002). *Semiconductor quantum dots: Physics, spectroscopy and applications*. Heidelberg: Springer-Verlag.

Metropolis, N., Rosenbluth, A. W., Rosenbluth, M. N., Teller, A. H., & Teller, E. (1953). Equations of state calculations by fast computing machines. *Journal of Chemical Physics*, *21*, 1087.

Merkt, U., Huser, J., & Wagner, M. (1991). Energy spectra of two electrons in a harmonic quantum dot. *Physical Review B*, *43* (9), 7320.

Molotkov, S. N., & Nazin, S. S. (2004). Quantum cryptography based on quantum dots . *JETP Letters*, *63*, 687.

Morelle, M., Bekaert, J., & Moshchalkov, V. V. (2004). Influence of sample geometry on vortex matter in superconducting microstructures. *Physical Review B*, *70*, 094503.

Nair, S. V., Sinha, S., & Rustagi, K. C. (1987). Quantum size effects in spherical semiconductor mycrocrystals. *Physical Review B*, *35*, 4098.

Nanofm Ltd. (n.d). *Quantum dot.* Retrieved 10 July, 2009, from http://www.nanofm.com/terms/quantum_dot.html

Ouellette, J. (2003). Quantum Dots for Sale. *The Industrial Physicist*, American Institute of Physics, 14.

Pozina, G. R., Kavokin, A. V., Kochereshko, V. P., Uraltsev, I. N., Yakovlev, D. R., Landwehr, G., Bicknell-Tassius, R. N., & Waag, A. (1992). Oscillator strength study of the 2D-3D exciton transition in CdTe/(Cd,Mn)Te quantum wells and superlattices. *Solid State Communications*, *81*, 639.

Popsueva, V. (2004). *Quantum dots a Monte Carlo simulation.* Oslo: Msc. Thesis.

Popsueva, V. *et.al.* (2005). Quantum and classical calculations of ground state properties of parabolic quantum dots. arXiv:cond-mat/0510185.

Pfannkuche, D., & Gerhardts, R. R. (1991). Quantum-dot helium: Effects of deviations from a parabolic confinement potential. *Physical Review B*, *44* (23), 13132-13135.

Pederiva, F., Umrigar, C. J., & Lipparini, E. (2000). Diffusion Monte Carlo study of circular quantum dots. *Physical Review B*, *62*, 8120.

Poole, C. P., & Owens, F. J. (2003). *Introduction to nanotechnology*, (1.st Edition). USA: WileyWiley-Interscience.

Que, W. (1992). Excitons in quantum dots with parabolic confinement. *Physical Review B*, *4*5, 11036.

Räsänen, E. (2004). *Electronic oroperties of non-circular quantum dots*. Espoo: Ph.D. Thesis.

Reynolds, P. J., Ceperley, D. M., Alder, B. J., & Lester, W. A. Jr. (1982). Fixed-node quantum Monte Carlo for molecules. *Chemical Physics*, *77*, 5593.

Reine, S. S. (2004). *Monte Carlo simulations of atoms*. Oslo: Msc. Thesis.

Reed, M. A. (1993). Quantum dots. *Scientific American, Inc*, 118.

Ruiz, M. B. (2004). Hamiltonian method for many-electon atoms. I. The Hamiltonian. *International Journal of Quantum Chemistry*, 101 (3), 246-260.

Siljamäki, S., Harju, A., Räsänen, E., Suorsa, J., & Nieminen, R. M. (2005). Diagonalizations on a C correlated basis. *Physica E*, *26*, 441.

Stébé, B., Munschy, G., Stauffer, L., Dujardin, F., & Murat J. (1997). Excitonic trion X^- in semiconductor quantum wells. *Physical Review B*, *56*, 12454.

Stedman, M. L. (1999). *Ground-state and finite temperature quantum Monte Carlo simulations of many-particle systems.* London: Ph.D. Thesis.

Stream Chemicals, Inc. (December 15, 2006). *Quantum dots - A definition, how they work, manufacturing, applications and their use in fighting cancer*. Retrieved 10 July, 2009, from http://www.azonano.com/Details.asp?ArticleID=1814

Şakiroğlu, S., Doğan, Ü., Yıldız, A., Akgüngör, K., Epik, H., Ergün, Y., Sarı, H., & Sökmen, İ. (2009). Ground state energy of excitons in quantum dot treated variationally via Hylleraas-like wavefunction. *Chinese Physics B*, *18*, 1578.

Şakiroğlu, S., Akgüngör, K., & & Sökmen, İ. (2009). Ground state energy of He isoelectronic sequence treated variationally via Hylleraas-like wavefunction. *Chinese Physics B*, (to be published).

Şakiroğlu, S. (2009). *Electronic S structure of quantum dots*. İzmir: Ph.D. Thesis.

Tsuchiya, S., Austing, D. G., Honda, T., van der Hage, R. J., & Kouwenhoven, L. P. (1996). Shell filling and spin effects in a few electron quantum dot. *Physical Review Letters 77*, 3613.

Tsuchiya, T. (2001). A quantum Monte Carlo study on excitonic molecules in type-II superlattices. *International Journal of Modern Physics B 15*, 3985.

Tan, M. Y. J., Drummond, N. D., & Needs, R. J. (2005). Exciton and biexciton energies in bilayer systems. *Physical Review B*, *71*, 0333033.

Tokura, Y. (29.12.200). *Configuration Interaction method for calculating energy spectrum of vertical quantum dots*. Retrieved February 15, 2008, from http://www.brl.ntt.co.jp/group/butsuden-g/tokura/ci/ci.html.

Taut, M. (1993). Two electrons in an external oscillator potential: Particular analytic solutions of a Coulomb correlation problem. *Physical Review A*, *48*, 3561-3566.

Thijssen, J. M. (2001). *Computational Physics*, (1.st Edition). UK: Cambridge University Press.

Towler, M. D. (2006). The Quantum Monte Carlo method. *Physica Status Solidi (b)*, *243*, 2573-2598.

Uozumi, T., Kayanuma, Y., Yamanaka, K., Edamatsu, K., & Itoh, T. (1992). Excited-state absorption of excitons confined in spherical quantum dots. *Physical Review B*, *59*, 9826.

Viega, J. (2003). Practical random number generation in software. *Proccedings of the 19th Annual Computer Security Applications Conference*, p.129.

Wikramaratna, R. (2000). Parallel random numbers. *SIAM News*, *33*, 1.

William, H., Flanerry, B. F., Teukolsky, S. A., Vetterling, W.T. (1992). *Numerical Recipies in Fortran 77: The Art of Scientific Computing*. (2.nd Edition). USA: Camridge University Press.

Williamson, A. J. (1996). *Quantum Monte Carlo calculations of electronic exitations*. Camridge: Ph.D. Thesis.

Xie, W. (2005). Exciton states trapped by a paraboplic quantum dot. *Physica B*, *358*, 109.

Yoffe, A. D. (1993). Low-dimensional systems: quantum size effects and electronic properties of semiconductor microcrstallites (zero-dimensional systems) and some quasi-two-dimensional systems. *Advances in Physics*, *42*, 173.